

Picoplanktonic methane production in eutrophic surface waters

Sandy E. Tenorio^{1, 2, 4}, Laura Farías^{1, 2, 3}

¹Departamento de Oceanografía, Facultad de Ciencias Naturales y Oceanográficas, Universidad de Concepción, Concepción, 4070043, Chile.

²Centro de Ciencia del Clima y la Resiliencia (CR2), Chile.

³Instituto Milenio en Socio-ecología Costera (SECOS), Chile.

⁴Programa de Graduados en Oceanografía, Departamento de Oceanografía, Universidad de Concepción, Concepción, 4070043, Chile.

Correspondence to: Laura Farías (laura.farias@udec.cl)

Abstract. Over the past decade, extensive research has delved into the methane (CH₄) paradox which involves aerobic CH₄ production. We present noteworthy observations of CH₄ oversaturation within the surface layer of the central Chile upwelling zone (36° S, 73° W) over two consecutive seasonal cycles (2018-2021). Complementing these observations, CH₄ cycling experiments were conducted, utilizing distinct plankton fractions (encompassing the natural planktonic community, fractions <150 μm, <3 μm, and <0.2 μm), in different productivity periods of phytoplanktonic production/composition throughout the year. Our findings underscore the pivotal role of picoplankton (<3 μm) in CH₄ production on the ocean surface, contrasting with the limited contribution of larger microorganisms (<150 μm). Notably, incubations with methylated substrates, such as methylphosphonic acid (MPn) and trimethylamine (TMA), induce heightened CH₄ production within the picoplanktonic fraction. This phenomenon is consistently observed during both upwelling (austral spring-summer) and non-upwelling (winter) seasons, with significance in the latter period, when *Synechococcus sp.* exhibits notably high relative abundance.

Long-term microcosm experiments highlight the crucial roles played by heterotrophic bacteria and cyanobacteria in methylotrophic methanogenesis. This process enhances CH₄ production, facilitated by the recycling of dissolved organic carbon (DOC). Picoplankton emerges as a pivotal factor influencing the recycling of methylated substrates, and it is responsible for maintaining CH₄ supersaturation. These findings provide valuable insights into the biogeochemical processes driving CH₄ dynamics, particularly in highly productive upwelling areas.

Key words: dissolved methane, surface methane production, picoplankton, coastal upwelling.

Key points:

1. Picoplankton plays a crucial role in maintaining CH₄ supersaturation in the surface layer under different oceanographic conditions, influencing its exchange with the atmosphere.
2. Methylated substrates, such as methylphosphonic acid (MPn) and trimethylamine (TMA), notably stimulate CH₄ production through picoplankton-mediated methylotrophic methanogenesis.
3. *Synechococcus sp.*, utilizing the MPn substrate during the non-upwelling season, and picoeukaryotes, utilizing the TMA substrate during the onset of upwelling, could emerge as crucial microorganisms involved in CH₄ generation.

38 1. Introduction

39 Methane (CH₄) is a short-lived yet potent greenhouse gas, exhibiting a significantly higher heat-trapping capacity than CO₂
40 over a century. Its importance lies in its substantial influence on global climate dynamics and the necessity for robust mitigation
41 strategies (IPCC, 2021; Harmsen et al., 2020). The ocean holds considerable amounts of dissolved and hydrate CH₄, rendering
42 its thorough study crucial for precise climate change modelling and comprehending its ecological diversification within
43 oceanic ecosystems (IPCC, 2021; Xu et al., 2022).

44 The distribution of CH₄ is intricately influenced by both complex physical (transport) and biogeochemical (production and
45 consumption rates) processes (Reeburgh, 2007). In the open ocean, surface waters generally display slight oversaturation,
46 whereas deeper waters tend toward equilibrium or undersaturation with respect to the atmosphere. However, there is often
47 CH₄ accumulation within the pycnocline (Lamontagne et al., 1973; Cicerone and Oremland, 1988; Holmes et al., 2000). These
48 distribution patterns led to the identification of the CH₄ paradox (see review Reeburgh, 2007). Early hypotheses have suggested
49 various sources for CH₄ oversaturation in the surface layer, including organic matter respiration within anoxic niches of
50 particulate organic material (Karl and Tilbrook, 1994), within fish (Oremland, 1979), and zooplankton guts (De Angelis and
51 Lee, 1994). However, these classical methanogenesis pathways remain obscured in the surface and oxic zone of aquatic
52 systems. Subsequent advancements in this field highlighted biochemical processes, such as methylotrophic methanogenesis,
53 now understood as the production of CH₄ from methylated compounds under diverse biogeochemical conditions (Karl et al.,
54 2008; Damm et al., 2010, 2015; Repeta et al., 2016).

55 Methylated compounds are synthesized or degraded by diverse autotrophic and heterotrophic microorganisms, for example,
56 *Nitrosopumilus maritimus* produces phosphonates like methylphosphonic acid (MPn) (Metcalf et al., 2012), whereas different
57 species of phytoplankton, in turn, contribute to sulphur derivatives such as methionine (Lenhart et al., 2016),
58 dimethylsulfoniopropionate (DMSP), dimethyl sulfide (DMS) (Belviso et al., 1990; Stefels and Van Boekel, 1993) and
59 trimethylamines (TMA) (Sun et al., 2019), serving as potential carbon sources for microorganisms and thereby contributing
60 to CH₄ generation via methylotrophic methanogenesis. Furthermore, there is a suggestion that photosynthesis plays a role in
61 direct CH₄ production (Berg et al., 2014; León-Palmero et al., 2020; Klintzsch et al., 2023). Several studies have shown
62 associations between CH₄ anomalies in surface waters and specific phytoplanktonic groups, such as coccolithophores (Lenhart
63 et al., 2016) and cyanobacteria (Bižić et al., 2020). Hence, recognizing phytoplankton in various size fractions as direct links
64 to CH₄ production in diverse marine ecosystems (Bizic, 2021), becomes imperative, especially through pathways involving
65 demethylation from methylated compounds (Damm et al., 2010; Florez-Leiva et al., 2013; Lenhart et al., 2016; Karl et al.,
66 2008; Sun et al., 2011; Repeta et al., 2016).

67 Coastal upwellings, due to their high productivity, represent an emblematic site for the study of CH₄ production, but the
68 proximity to anoxic sediments and prevalent anaerobic methanogenesis in sediments or in the oxygen minimum zones (OMZ)
69 often obscures the study of CH₄ generation within oxygen-rich surface waters. Indeed, CH₄ profiles predominantly exhibit
70 significant increases towards anoxic sediments (Fariás et al., 2021; Ma et al., 2020; Kock et al., 2008). Coastal regions serve

71 as intensive CH₄ sources, facilitating lateral transport to open waters (Borges and Abril, 2012; Upstill-goddard and Barnes,
72 2016) and/or the atmosphere due to vertical advection linked to coastal upwelling (Farías et al., 2021; Kock et al., 2008).
73 Current global CH₄ balances exhibit high uncertainty (Saunois et al., 2020; Roth et al., 2022; Lu et al., 2021) and considerable
74 spatial/temporal variability, particularly in coastal environments, where fluxes represent over 40% of total atmospheric fluxes
75 (Weber et al., 2019; Bange et al., 1994).

76 Given the upwelling systems are expected to integrate all before mentioned mechanisms, investigating CH₄ dynamics becomes
77 pivotal. Upwelling processes dynamically transport nutrient-rich water onto continental shelves and surface, significantly
78 enhancing biological productivity to eutrophic levels. This surge in high microbial productivity, biomass, and organic matter
79 decomposition, establishing these areas as pivotal hubs for carbon cycling, particularly in CH₄ (Capone and Hutchins, 2013).
80 Indeed, in upwelling systems a large part of the primary production is channelled to dissolved organic carbon (DOC) through
81 the microbial food web, and a less percentage directly to copepods via the herbivore food chain (Vargas et al., 2007). In
82 addition, coastal areas receive large amounts of DOC from rivers (Bianchi, 2011), this is also the case of upwelling systems
83 off central Chile (Vargas et al., 2013). These microbial food web and riverine pathways not only transport and remineralize
84 nutrients and DOC but also fosters the generation of greenhouse gases like CH₄ (Dinasquet et al., 2018; Sun et al., 2019).

85 Crucially, specific microbial groups such as Pelagibacter, SAR 11, among other, considered key players in DOC recycling,
86 have been identified as potential contributors to CH₄ regeneration from diverse C-1 compounds (Carpenter et al., 2012; Repeta
87 et al., 2016; Sun et al., 2019). The synergy between autotrophic (e.g., picoeukaryotes, cyanobacteria) and heterotrophic
88 picoplankton (<3 µm) could represent pathways for CH₄ production in coastal regions. Therefore, the main aim of this study
89 is to investigate the dynamics of CH₄ oversaturation within the surface layer of the central Chile upwelling zone using
90 observational and experimental approaches. Among objectives are to discern the contributions of different plankton fractions,
91 particularly picoplankton and to unravel the involvement of methylated substrates like MPn and TMA in stimulating CH₄
92 production. Ultimately, this research will provide comprehensive insights into the biogeochemical mechanisms that drive CH₄
93 dynamics within highly productive upwelling water, emphasizing the role of picoplankton in maintaining CH₄ oversaturation
94 in the surface ocean.

95 **2. Material and methods**

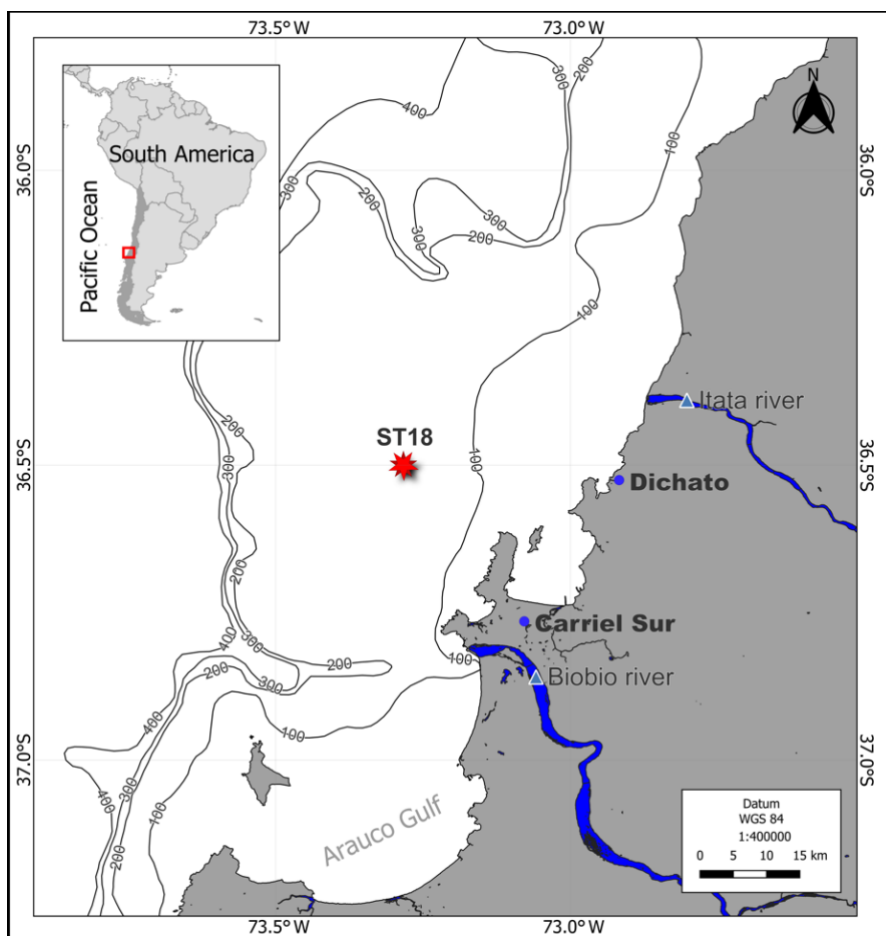
96 **2.1 Regional setting.**

97 The continental shelf off central Chile undergoes wind-driven coastal upwelling, seasonally controlled by the migration of the
98 South Pacific anticyclone (Strub et al., 1998). This process leads to alongshore equatorward winds during the summer- spring
99 period, producing coastal upwelling (Sobarzo and Djurfeldt, 2004; Sobarzo et al., 2007). The area is influenced by Equatorial
100 Subsurface Water (ESSW), which is nutrient rich and has low dissolved O₂ levels (less than 44 µM). The ESSW interacts with
101 sediments and serves as a nutrient source during coastal upwelling, delivering low O₂ concentrations and high organic matter

102 content to the bottom water and sediments, fostering anaerobic organic matter mineralization supporting denitrification,
103 sulphate reduction and methanogenesis (Ferderlman et al., 1997; Farías et al., 2004).

104 2.2 Water collection.

105 Seawater was collected from the upwelling zone of central Chile ($36^{\circ} 0.802' S$; $73^{\circ} 07.750' W$) at the University of
106 Concepcion's time series station (ST18), situated at a depth of 90 meters (Fig. 1). Monthly samplings have been conducted
107 aboard the RV Kay Kay II since 2002. Continuous sampling with a CTD-O (SBE-19) instrument was performed to obtain
108 temperature, salinity, and dissolved oxygen (DO) profiles, whereas seawater samples using 10 L Niskin bottles at various
109 depths (0, 5, 10, 20, 30, 50, 65 and 80 m) were obtained in triplicate for dissolved gas (DO and CH_4), nutrient and chlorophyll-
110 a (Chl-a) analysis. Detailed methodologies can be found in Farías et al. (2021). From March 2019 to June 2020, DOC samples
111 were specifically procured from depths of 5, 20, 50 and 80 m.



112
113 **Figure 1. Time series location map (ST18) over the central Chile upwelling platform. The Itata and Biobio rivers, Carriel sur**
114 **meteorological station and Dichato town are indicated.**

115 To investigate the role of different sized planktonic communities in CH₄ cycling, seawater was gathered at a depth of 10 m,
 116 a depth commonly associated with the Chl-a peak (Testa et al., 2018). Large zooplankton (150 µm mesh sieve) were excluded
 117 using the methodologies outlined by Sieburth et al. (1978). The experimental setup is outlined in Table 1 and includes two
 118 negative controls: 1) sterile filtration using a 0.2 µm filter, often-used method for the removal of microorganisms (Hahn, 2004),
 119 and 2) poisoning with the addition of HgCl₂ to ensure total inactivation of few bacterial species which can pass through 0.2-
 120 microm filters (Hahn, 2004). The positive control was the natural community (NC) without any filtration.

121 Another set of experiments enriched with the organic methylated substrates MPn and TMA were performed using only the
 122 fractionated picoplanktonic community. To maintain the integrity of the samples, seawater was transported in dark and
 123 refrigerated drums placed inside expanded polystyrene boxes surrounded by ice packs to preserve the natural temperature of
 124 the seawater (~13°C) and minimize microbial activity. The average time for transportation to the Marine Station Biology
 125 Laboratory at Dichato was approximately 4 hours. However, it is important to note that there were delays of 8 to 12 hours
 126 between arrival at the laboratory and the onset of short- and long-term experiments, respectively. These delays were due to
 127 filtering and a short acclimatization process (6 hours) required before initiating the experiments, but these procedures were
 128 done in cool room (13°C).

129 This is a time series study, from 2018 until 2021, encompassing CH₄ regeneration in different productivity phases (Table 1)
 130 according to (Testa et al., 2018). In this regard, two types of experiments described in the following sections will be conducted.

131 **Table 1. Summary of the experimental setup of short-term (GC vials) and long-term (microcosms) experiments with different**
 132 **treatments: NC: seawater with the natural plankton (control); <3 µm: picoplankton; <0.2 µm: femtoplankton (control +); <0.2 µm**
 133 **+ HgCl₂: femtoplankton with HgCl₂ (control +) and CC: picoplankton concentrate; and the addition of methylated substrates (MPN:**
 134 **methyl phosphonic acid and TMA: trimethylamines). Different phases of the productivity period are: PI: Phase I; PII: Phase II;**
 135 **and PIII: Phase III.**

Date	Type of experiment	Setup	Plankton size (µm)	Place	Time (h)	Productivity period
December 2018	GC vials	Plankton fractionation	CN, <3 and <0.2	Incubator	24	High (PI)
January 2019	GC vials	Plankton fractionation	CN, <3 and <0.2	Incubator	24	High (PI)
March 2019	GC vials	Add: MPn	<3	Incubator	24	Intermediate (PII)
May 2019	GC vials	Add: MPn and TMA	<3	Incubator	24	Basal (PIII)

April 2019	Microcosms	Add: MPn and TMA	CN, <3, and CC	Cold room	~ 60	Intermediate (PII)
September 2019	Microcosms	Add: MPn and TMA	CN, <3, and CC	Cold room	~ 60	High (PI)

136

137 **2.3 Short-term experiments of CH₄ cycling from size-fractionated planktonic community enriched with organic**
138 **substrates.**

139 The size fractionation of planktonic communities was conducted through a careful sequential filtration process, where 5 L of
140 seawater was gently passed through a pre-filter of 150 µm nylon, followed by 3 µm Isopore, and 0.22 µm Millipore membranes,
141 yielding two fractions: picoplankton (<3 µm), and femtoplankton (<0.2 µm) communities; the last one used as a negative
142 control in some experiments. NC was obtained directly without filtering (Table 1).

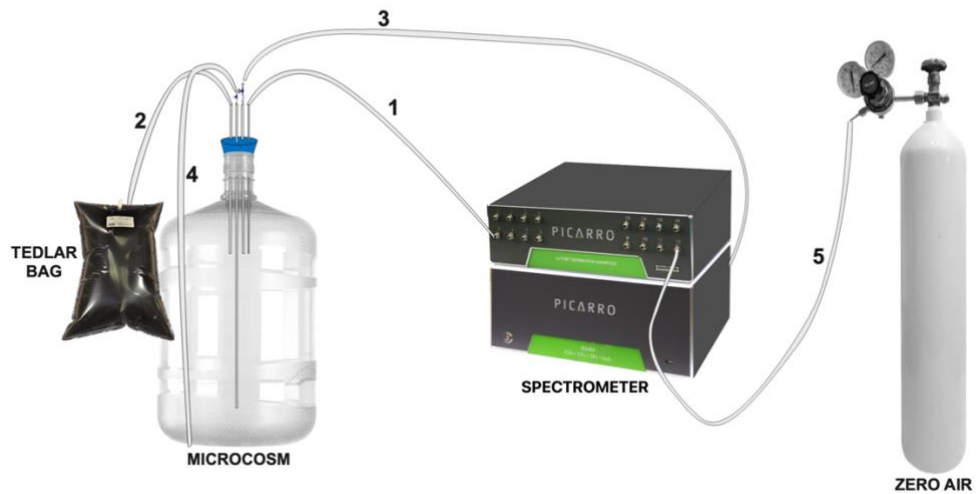
143 Prior to incubation, initial seawater sampling was taken for each treatment group, wherein triplicate measurements were taken
144 of DO (125 mL), COD (60 mL), Chl-a (100 mL), and nutrients (15 mL). Subsequently, each size-fractionated sample was
145 homogenized and swiftly transferred into 20 mL vials (108 in total, twenty-seven per treatment). These vials were immediately
146 sealed using rubber and aluminium caps to prevent any potential atmospheric gas contamination. The incubation of these vials
147 took place within an FOC 225E incubator, maintained at a temperature of 13 °C, and under a 12-hour photoperiod (24 hours).

148 The illumination was calibrated to fall in a range of 11-11.5 µmol m⁻² s⁻¹ using blue and neutral density blank filters. At
149 intervals of four hours, three vials from each treatment (Table 1) were withdrawn, and immediately poisoned with 50 µL of
150 HgCl₂ and then, the vials were gently agitated to ensure homogenization. Gas chromatography was employed to analyze the
151 CH₄ content of the vials. In another set of experiments (Table 1), the picoplankton fraction was singled out to ascertain its
152 capacity for metabolizing methylated substrates and subsequently regenerating CH₄. This involved adding MPn and TMA to
153 the samples. The final concentration of both substrates in these treatments was maintained at 1 µM, assuming that natural
154 concentrations in the seawater were at trace levels. Thus, these could be considered as potential experiments (highly enriched).
155 The experimental conditions remained consistent with those employed in the earlier experiment.

156 **2.4 Long-term experiments of CH₄ cycling from size-fractionated planktonic community enriched with organic**
157 **substrates.**

158 Nine microcosms were developed using a system of gas-tight polycarbonate bottles (13 L). Each microcosm contained 10L of
159 seawater for treatment and 3L of headspace. They were equipped with a closed gas circuit and connected to a gas spectrometer
160 analyzer capable of simultaneously and continuously measuring various gases, including CO₂, CH₄, N₂O, and humidity
161 percentage (Fig. 2). Each bottle featured a rubber cap equipped with four holes (as depicted in Fig. 2), housing a 5mm glass
162 capillary within each hole. These capillaries were connected to gas-tight Teflon hoses. Specifically, the first capillary extended

163 to the middle of the headspace (1) and was linked to an accessory (16-Port Distribution Manifold A0311) of the Picarro G-
164 2308 spectrometer for Cavity Ring Spectroscopy System (CRDS), designed for the measurement of gases in equilibrium with
165 the aqueous phase. The second capillary was suspended within the headspace (2) and connected to a Tedlar bag (3 L) filled
166 with N₂. This arrangement aimed to prevent imbalance when drawing water samples from the microcosm. The third capillary,
167 also suspended in the headspace (3), was equipped with a 3-way cannula, and was connected to the air outlet of the Picarro G-
168 2308 spectrometer, to facilitate the recirculation of air within the headspace. This system optimization aimed to mitigate
169 excessive headspace during spectrometer air sampling, preventing a gas-seawater phases imbalance. This hose (3) was
170 adjustable and replaced upon measuring gas concentrations in each microcosm. The fourth glass capillary was submerged in
171 the seawater, 3 cm from the bottom (4). It was attached to a 3-way cannula, streamlining the sample extraction process.



172
173 **Figure 2. Assembly of the microcosm for long-term experiments (10 L). Capillary 1 is connected directly to the spectrometer.**
174 **Capillary 2 is connected to a TEDLAR bag filled with N₂ (3L). Capillary 3 is removable and connected to the outlet of the**
175 **spectrometer. Capillary 4 is connected to a loose hose for water sampling and hose 5 is connected to zero air.**

176 In both April and September of 2019, a series of long-term microcosm experiments were conducted. These months were
177 strategically chosen: the first coinciding with the transition of phytoplankton composition to nano-picoplankton (basal
178 productivity period), and the second with diatom blooms (larger phytoplankton dominance) (high productivity period), as
179 highlighted in studies by Anabalón et al. (2007) and Cuevas et al. (2004). The experiment encompassed three distinct
180 treatments, 1) Control without any methylated substrates addition in natural communities (NC), picoplankton community (<
181 3 μm) and concentrated picoplanktonic community (CC) 2) all treatments enriched with MPn 3) and all treatments enriched
182 with TMA (see Table 1).

183 The concentrated fraction of picoplankton (CC) was procured through tangential flow filtration via a 0.2 μm filter, following
184 a procedure developed by Giovannoni et al. (1990) for harvesting greater quantities of microbial biomass and using pre-

185 filtering steps as discussed earlier to concentrate only picoplankton ($<3 \mu\text{m}$). To discern whether the tangential flow filtering
186 was effective, the abundance of cyanobacteria, picoeukaryotes and heterotrophic bacteria was measured with flow cytometry.
187 The incubations were carried out within a controlled cold room environment, maintaining a temperature range of 12 to 13 °C,
188 with same illumination used in short periods over 60 hours. In the initial stages, each bottle was sealed and allowed to acclimate
189 for six hours in darkness. Following this stage, 1 mL of MPn (10 mM stock solution) and TMA (10 mM stock solution) were
190 introduced to each bottle, yielding a final concentration of 1 μM , matching the conditions established in prior experiments.
191 To prevent CH_4 residue contamination, a purge with Zero air was performed (as shown in Fig. 2, line 5), ensuring accurate
192 CH_4 concentration measurement within each microcosm, and establishing a baseline. Every four hours a cycle of CH_4
193 measurements was conducted continuously over 3 minutes, followed by a 6-minute hose cleaning (used for recirculation) with
194 Zero air before connecting to capillary 3 for subsequent measurement. It is important to note that the equipment absorbed 240
195 mL of air per minute of reading. Therefore, air recirculation within the microcosm, as previously mentioned, was essential.
196 Preceding the actual experiment, the concentrations of gases measured by the spectrometer were closely monitored for 30
197 minutes, confirming that the recirculation process did not impact the measured gas concentrations.

198 **2.5 Chemical and biological analysis.**

199 **2.5.1. Dissolved methane.**

200 Once the CH_4 samples were taken, they were stored upside down, at room temperature and protected from light, and then
201 analyzed in the GC. CH_4 (discrete samples) was determined using the phase equilibrium method (McAuliffe, 1963). In this
202 procedure, each vial was carefully treated, with the addition of 5 mL of inert gas (helium), creating a headspace to facilitate
203 equilibrium between the aqueous and gas phases. Subsequently, the gas phase was measured into a gas chromatography
204 Shimadzu 17 equipped with a flame ionization detector (FID). A Restek RT QS-Bond column (30 m length, 0.53 mm inner
205 diameter, 20 μm film thickness) was employed, maintained at a temperature of 30 °C with a flow of 2.6 ml min^{-1} , using He as
206 an ultrapure gas carrier.

207 Five-point calibration curves (linear response of the detector) were made for each monthly sample set (treatment), using a gas
208 with a composition and concentration equivalent to that of the current atmosphere from NOAA (1863.4 ± 0.3 ppbv for CH_4)
209 (Bullister et al., 2016) as the primary standard, as well as three standard gas mixtures (Air Liquide, USA) and zero air (synthetic
210 air without CH_4 tracers). In each CH_4 sample set (every treatment), standards were added at the beginning, middle and end of
211 the measurements to corroborate the correct functioning of the detector. CH_4 measurements (triplicate) with a variation
212 coefficient greater than 10% were not considered.

213 **2.5.2. Dissolved oxygen.**

214 To assess DO content, 125 mL glass flasks were used for sample collection in triplicate. These samples were immediately
215 fixed and analyzed within 6 hours of collection through the Winkler method (Carpenter, 1965). The analysis was conducted

216 using a Dosimat 665 instrument featuring an automatic photometric endpoint detector. The detection limit for this method
217 stood at 2 $\mu\text{mol L}^{-1}$.

218 **2.5.3. Nutrient.**

219 Nutrient samples were collected in triplicate using a 60 mL syringe and filtered through a 0.45 μm cellulose acetate filter. The
220 filtered content was held in 15 mL Falcon polyethylene bottles and stored at -20°C . Analysis of these nutrient samples followed
221 standard colorimetric techniques (Grasshoff et al., 1983) and was conducted using a SealAA3 segmented flow auto-analyzer.
222 This analyzer featured four distinct channels, each equipped with specific modules tailored for individual nutrients.

223 **2.5.4. Chlorophyll-a.**

224 To quantify Chl-a content, triplicate samples of 100 mL seawater were filtered using a GF/F filter and immediately stored at -
225 20°C . Analysis was performed according to the method outlined by (Holm-Hansen et al., 1965). A Turner Designs 10AU
226 fluorometer was employed for measurement, and a standard pigment served as a reference (Sigma-Aldrich C6144-1MG).

227 **2.5.5. Dissolved Organic Carbon.**

228 For DOC assessment, samples were collected in triplicate using polyethylene bottles. Each 60 mL seawater sample was filtered
229 through a GF/F filter that had been pre-treated by heating at 450°C for 4 hours. After filtration, the samples were acidified to
230 achieve a pH range of 2-3 and stored at -20°C . Analysis of these samples involved the infrared combustion method using a
231 Shimadzu Organic Carbon Analyzer (TOC-LCPH).

232 **2.5.6. Cytometry.**

233 For picoplankton abundance, 3mL of water was fixed with a glutaraldehyde solution (1%) and promptly frozen (-80°C) in
234 liquid nitrogen for storage. Samples were analyzed with flow cytometry using an INFLUX, Cytopeia, equipped with five lasers
235 (355-457-488-532-638 nm). Sort gates were optimized based on the autofluorescence of each group. *Synechococcus sp.* were
236 identified based on their orange fluorescence (530/40 nm) using 488 nm blue and 532 nm green lasers, picoeukaryotes were
237 identified by their red fluorescence (692/40 nm) using 488 nm blue laser, and bacterioplankton were detected using a
238 combination of side scatter light (SSC) (related to cell size) versus green fluorescence (530/40 nm).

239 **2.6 Data analysis.**

240 **2.6.1. Dissolved methane.**

241 Dissolved CH_4 concentration was calculated using the solubility coefficient from Wiesenburg and Guinasso (1979). The water
242 column was divided into two layers according to density gradients: (1) surface layer (0 - 20 m) well mixed and (2) subsurface
243 layer (20 – 90m) from the base of the mixed layer to the bottom, around ~ 90 m (Farías et al., 2015), this was to interpret the
244 vertical and temporal variability of CH_4 variation.

245 CH_4 dissolved in the microcosms were measured using continuous sampling connected to the spectrometer CRDS. To convert
246 CH_4 concentrations from molar dry phase to dissolved concentrations the Wiesenburg and Guinasso (1979) solubility

247 coefficient, calculated from the *in-situ* T and S, was used. Each time in the microcosm experiment represents the average of
248 the plateau of each measurement (around 150 and 200 measurements, approximately).

249 **2.6.2. Methane saturation.**

250 CH₄ saturation was calculate following Eq. (1):

$$251 \text{ Sat}(\%) = \frac{[CH_4]_{in\ situ}}{[CH_4]_{eq}} \quad (1)$$

252 Where [CH₄]_{eq} was calculated using solubility coefficient from Wiesenburg and Guinasso (1979).

253 **2.6.3. Methane anomalies and methane hot moments.**

254 Monthly anomalies of CH₄, were estimated only in the surface layer, using the following Eq. (2):

$$255 \text{ Anomaly} = \frac{xCH_4 - \bar{x}CH_4}{\sigma_{CH_4}} \quad (2)$$

256 Where: xCH₄ is the discrete value at a certain depth (surface) and time (month), and $\bar{x}CH_4$ is the median value for the whole
257 (2018-2021) period at surface and σ_{CH_4} is the standard deviation of this dataset. CH₄ hot moments were defined as a ΔCH_4
258 three times higher than the average monthly of anomaly ($\bar{x} \Delta CH_4$) at each depth within the surface layer as Eq. (3):

$$259 \frac{\Delta CH_4}{\bar{x} \Delta CH_4} > 3 \quad (3)$$

260 Where: ΔCH_4 is the disequilibrium of this gas at each depth and was estimated as Eq. (4):

$$261 \Delta CH_4 = [CH_4]_{in\ situ} - [CH_4]_{eq} \quad (4)$$

262 **2.6.4. Inventories.**

263 Inventories of CH₄, Chl-a and nutrients at the surface (SL) and illuminated layer and subsurface and dark layer (SSL) were
264 calculate through the trapezoidal integration of concentrations of each variable at every layer; minimum three depths in each
265 layer. The averages were taken for DOC, because there were only two measurements in each layer.

266 **2.6.5. Methane recycling rates.**

267 The net CH₄ recycling rate (net CH₄ accumulation minus CH₄ consumption) in different fractions of the phytoplankton
268 community was calculated through a linear regression of CH₄ concentrations (Farías et al., 2009) during the incubation time
269 (24 hours), separating the light cycles (12 hours of light and 12 hours of darkness).

270 **2.6.6. Methane fluxes.**

271 The daily CH₄ flux ($F = \mu\text{mol m}^{-2} \text{ d}^{-1}$) across air-sea interface was determined using the equation from Broecker and Peng
272 (1974), modified by Wanninkhof (1992) as follows Eq. (5):

$$273 F = K_w * (C_w - C^*) \quad (5)$$

274 Where: K_w (cm h⁻¹) is the transfer velocity from the surface water to the atmosphere, as a function of wind speed, temperature,
275 and salinity from the mixed layer depth (MLD), where wind speed were obtained from a meteorological station located at
276 Carriel Sur (<http://www.meteochile.gob.cl/>) and MLD was calculated using a potential density-based criterion of Kara et al.
277 (2003). C_w (nmol L⁻¹) is the mean CH₄ concentration in the mixed layer and C^* is the gas concentration in the mixed layer
278 expected to be in equilibrium with the atmosphere according to Wiesenburg and Guinasso (1979). Historical atmospheric

279 values were obtained from registers of gas hemispheric and global monthly means from the NOAA/ESRL program at NOAA
280 (<http://www.esrl.noaa.gov>). More details about the calculation of CH₄ fluxes in Farías et al. (2021).

281 **2.6.7. Brunt-Väisälä frequency (BVF).**

282 The Brunt Vaisala frequency was derived from the observed pressures, temperatures and salinities for each depth set using the
283 TEOS-10 equation of state. This was done in Ocean Data View (ODV v5.6.4) software. Negative values indicate unstable
284 conditions (Schlitzer, 2023).

285 **2.7 Statical analysis**

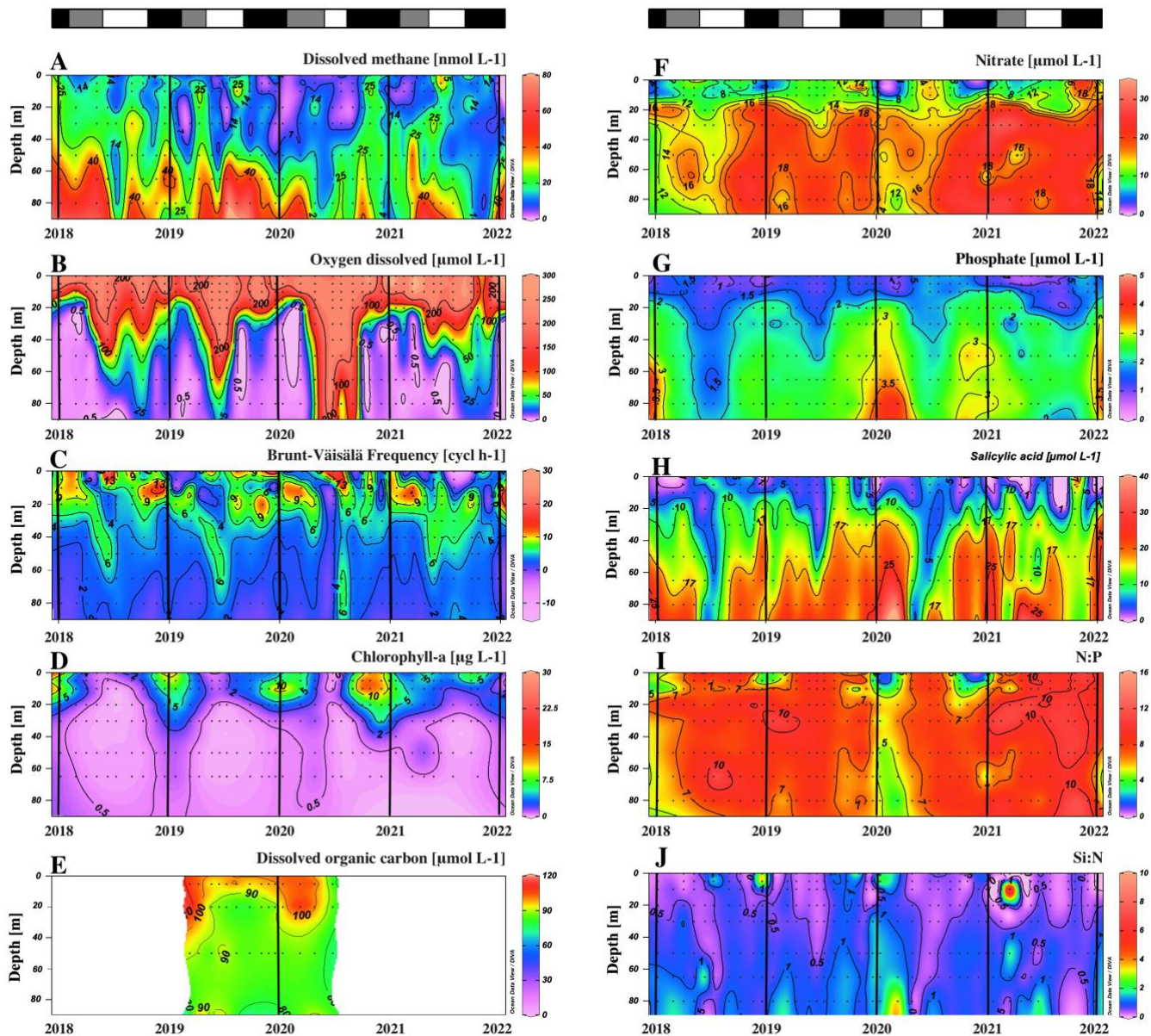
286 To determine significant differences between the upwelling and non-upwelling periods in both surface and subsurface layers,
287 the non-parametric Mann-Whitney U test was used. To analyse the degree of relationship between oceanographic variables
288 and the variability of CH₄ in the surface layer, Spearman correlations were used. Also, to identify patterns surface and
289 subsurface variation, a Principal Component Analysis (PCA) was performed. In addition, the Kruskal-Wallis non-parametric
290 statistical test was used to define significant differences between the concentrations given by the different treatments. The
291 value statistically significant was considered as $p < 0.05$.

292 **3 Result and discussion**

293 **3.1 Oceanographic characteristics related to wind-driven coastal upwelling in central Chile.**

294 Figure 3 shows the seasonal variability of DO, stratification, Chl-a, DOC, nutrients, and their ratios. Coastal areas off central
295 Chile have a well-documented seasonality of upwelling favourable winds (Strub et al., 1998). Previous studies, based on wind
296 forcing, have identified two distinct seasons: spring-summer (September to April) upwelling and fall-winter (May to August)
297 non-upwelling (Sobarzo et al., 2007). This seasonality significantly influences temperature, salinity, DO, nutrients, and surface
298 Chl-a concentrations in response to wind-driven stress (Strub et al., 1998; Aguirre et al., 2012). Notably, although most
299 oceanographic variables have clear seasonal patterns, a comparatively weak seasonality is observed in dissolved CH₄ (Fig.
300 3A).

301



302

303

304

305

306

307

308

309

310

311

Figure 3. Time series of vertical distributions of A. Methane (nmol L^{-1}), B. Dissolved oxygen ($\mu\text{mol L}^{-1}$), C. Brunt-Vaisala Frequency (cycl h^{-1}), D. Chlorophyll-a ($\mu\text{g L}^{-1}$), E. Dissolved Organic Carbon (no Purgeable Organic Carbon - μM), F. Nitrate ($\mu\text{mol L}^{-1}$), G. Phosphate ($\mu\text{mol L}^{-1}$), H. Salicylic acid ($\mu\text{mol L}^{-1}$), N:P ratio and J. Si:N ratio. Sampling was made at ST18 from January 2018 to December 2021. Black lines indicate the start of each year (January). The top bars show different periods primary production, in black is a high productivity period (Phase I), in gray is an intermediate productivity period (Phase II), and in white is a low productivity (Phase III).

In the subsurface layer, CH_4 concentrations range from 0.43 to 78.72 nM (mean \pm SD = 23.44 ± 15.38 nM, Fig. 3A). These elevated levels could be associated with the seasonal dynamics of organic matter mineralization under hypoxic and suboxic

312 conditions during the upwelling period (spring-summer) (Brown et al., 2014; Capelle and Tortell, 2016; Kock et al., 2008;
313 Farías et al., 2021); however, there are no significant differences in CH₄ accumulations ($p = 0.40$) in subsurface waters during
314 the upwelling (mean \pm SD = 22.52 ± 14.34 nM) and non-upwelling (mean \pm SD = 24.60 ± 16.65 nM) periods (Fig. 3A).
315 Previously, long-term CH₄ climatology has observed similar values in surface and subsurface layers (Farías et al., 2021).
316 In the surface layer, there is a highly heterogeneous distribution of CH₄ concentrations, ranging from 0.14 to 41.72 nM (mean
317 \pm SD = 11.70 ± 7.79 nM). There are brief events of high CH₄ accumulations within water column, known as “hot moments”
318 (McClain et al., 2003; referring to disproportionate accumulations over time). CH₄ concentrations during hot moments are
319 between 10.17 nM (390% saturation) and 41.72 nM (1650% saturation) and persist during upwelling and non-upwelling
320 periods, as observed in Fig. S1 and Fig. S2. Persistently high CH₄ concentrations in mixing layer depth results in substantial
321 CH₄ effluxes, varying between 3.35 and 23.42 $\mu\text{mol m}^{-2} \text{d}^{-1}$ (mean \pm SD = 10.10 ± 5.77 $\mu\text{mol m}^{-2} \text{d}^{-1}$). When effluxes are
322 estimated and compared for upwelling and non-upwelling periods, there are not significant differences. The lack of seasonal
323 differences in mean surface CH₄ concentrations ($p = 0.63$) and effluxes ($p = 0.23$) could indicate additional input sources, such
324 as river discharges or local surface production. Potentially, the Itata River may contribute to CH₄, DOC and chromophoric
325 DOM (CDOM) discharge (Bello, 2016; Vargas et al., 2016; Rain-Franco et al., 2019); stimulating CH₄ production through
326 aerobic methanogenesis and photooxidation processes (Li et al., 2020; Zhang and Xie, 2015).
327 CH₄ profiles from samples are shown in Figure S2. Specific dates present peaks in surface CH₄ over different concentrations,
328 occasionally presenting levels exceeding those in the subsurface layer; so, it is understood that these hot moments in the surface
329 layer are not associated with the vertical advection of CH₄-rich bottom waters.
330 Thus, it is considered whether hot moments result from physical processes, such as vertical and/or advection associated with
331 upwelling and river discharge, respectively, or biological microbial processes. For the latter, hot moments might be due to *in*
332 *situ* aerobic methanogenesis, a process related to the growth and metabolic activities of microalgae (Günthel et al., 2020;
333 Hartmann et al., 2020; Del Valle and Karl, 2014; Bizic, 2021; Cerbin et al., 2022) and bacteria (Repeta et al., 2016; Metcalf
334 et al., 2012; Sun et al., 2019). This type of production is suggested to be a significant reason for CH₄ fluxes in various aquatic
335 systems, including stratified lakes (Grossart et al., 2011; Günthel et al., 2019; Wang et al., 2018), and open oceans (Damm et
336 al., 2010; Karl et al., 2008; Repeta et al., 2016; Sosa et al., 2020; Ye et al., 2020).
337 Relatively high Brunt-Väisälä frequency (BVF) values (>10 cycl/h) are observed between depths of 0 and 20 m, particularly
338 from September to December (Fig. 3C), whereas subsurface BVF values seem to be associated with annual patterns of thermal
339 stratification, where upwelling from the nearly homogenous ESSW between October and April leads to high density
340 homogeneity and lower BVF values. During fall and winter, elevated BVF values are observed in surface waters, probably
341 due to discharge from the Itata river; remarkably there are notably stable values in the subsurface layer (Fig. 3C).
342 The upper 20 m of the water column has Chl-a concentrations above 10 $\mu\text{g L}^{-1}$ (with a marked subsurface peak over different
343 depths) (mean \pm SD 6.60 ± 5.98) in September to January (spring-summer); while lower and more homogeneous values
344 (ranging from 0.5 to 1 $\mu\text{g L}^{-1}$) are detected during late summer (February to April, mean \pm SD 3.23 ± 2.87), fall and winter
345 (May to August, mean \pm SD 1.36 ± 1.91) (Fig. 3D). The study area presents typical DOC concentrations, as expected for

346 highly productive coastal zones (Igarza et al., 2019; Vargas et al., 2013), ranging from 58.79 to 128.63 μM (mean \pm SD =
 347 90.37 ± 17.05) with peak DOC concentrations during late summer and early fall (Fig. 3E). The surface layer shows reduced,
 348 but not depleted nutrient concentrations, whereas the subsurface layer presents consistently higher nutrient concentrations (Fig.
 349 3F–H). Within the upper 10 m depth, minimum mean NO_3^- and PO_4^{3-} concentrations occur from September to January, and
 350 intermediate and higher values between February and August (Fig 3 F-G). These trends are consistent with plankton temporal
 351 dynamics (see below). In contrast, Si(OH)_4 exhibits higher but heterogeneous concentrations during late autumn and winter,
 352 and lower values during spring and summer (Fig. 3H). This pattern reflects the high levels of Si(OH)_4 associated with river
 353 discharges in winter and the development of diatom blooms in spring and summer. CH_4 hot moments occur consistently
 354 throughout the year with different stratification scenarios in the water column (Fig. 3A and C), and with different Chl-a levels
 355 (Fig. 3D), revealing a complex interaction between substrates (nutrients and DOC), involved microorganisms and
 356 environmental factors (e.g. light, nutrients, water column stability).

357 Three distinct periods or phases of annual productivity are considered within the study area, based on existing data of primary
 358 production, phytoplankton biomass, and phytoplankton succession (i.e. changes in composition), related with other biophysical
 359 variables (Testa et al., 2018). These periods are; September to January (Phase I), with high productivity and Chl-a biomass,
 360 dominated by microplankton including large diatoms, tintinids, and dinoflagellates; from February to April (Phase II) with
 361 intermediate productivity, characterized by a shift in plankton composition biomass from larger to smaller organisms, such as
 362 flagellates; and from May to August (Phase III), with basal level productivity and relatively low Chl-a biomass, which
 363 corresponds to a non-upwelling period, with a prevalence of pico and nanoplankton (e.g., *Synechococcus*) including small
 364 flagellates and ciliates.

365 Table 2 presents inventories on CH_4 , Chl-a, DOC, NO_3^- , PO_4^{3-} , Si(OH)_4 , and inorganic nutrient ratios (N:P and Si:N) observed
 366 in these periods. The data on Chl-a indicates a marked variation, decreasing from spring to winter (Table 2).

367 **Table 2. Average inventories of biogeochemical variables: methane ($\mu\text{mol m}^{-2}$), chlorophyll-a (mg m^{-2}), DOC ($\mu\text{mol m}^{-2}$), nitrate**
 368 **($\mu\text{mol m}^{-2}$), phosphate ($\mu\text{mol m}^{-2}$), silicate ($\mu\text{mol m}^{-2}$), N:P and Si:N ratios, estimated for each productivity period (mean \pm SD) from**
 369 **2018 to 2021. These inventories are estimated for surface layer (SL) and subsurface layer (SSL). Number of hot moments in each**
 370 **period are counted. Phase I: September to January. Phase II: February to April. Phase III: May to August.**

Variable	Layer	Productivity periods		
		High	Intermediate	Basal
		Phase I (spring-summer)	Phase II (summer-autumn)	Phase III (autumn-winter)
CH_4	SL	265.59 ± 58.36	162.35 ± 21.44	240.54 ± 78.97
	SSL	1315.07 ± 173.69	1012.86 ± 163.23	1275.17 ± 286.38
Chl-a	SL	154.4 ± 102.31	51.32 ± 31.02	26.19 ± 21.17
DOC	SL	114.44 ± 53.94	112.88 ± 8.36	92.41 ± 11.27

	SSL	100.35 ± 46.51	96.97 ± 23.78	86.12 ± 8.95
NO ₃ ⁻	SL	260.61 ± 96.25	208.67 ± 49.51	224.65 ± 13.44
	SSL	1274.41 ± 344.24	1033.51 ± 38.5	987.6 ± 113.58
PO ₄ ⁻³	SL	38.08 ± 10.35	30.29 ± 3.51	28.16 ± 2.99
	SSL	170.22 ± 34.07	137.05 ± 21.57	119.38 ± 11.73
Si(OH) ₄	SL	131.75 ± 47.07	91.65 ± 38.68	111.24 ± 37.9
	SSL	1065.32 ± 206.98	811.2 ± 225.51	678.07 ± 168.68
N:P	SL	7.69 ± 2.57	7.59 ± 2.44	8.48 ± 0.55
	SSL	9.28 ± 2.52	8.24 ± 0.92	8.46 ± 0.84
Si:N	SL	0.67 ± 0.1	0.69 ± 0.73	0.49 ± 0.15
	SSL	1.04 ± 0.08	1.01 ± 0.26	0.74 ± 0.11
Hot moments	SL	19	9	15

371

372 Notably, surface data on DOC shows a marginal reduction from Phase I to Phase III (Table 2). It is possible that this fluctuation
373 in DOC accumulation/depletion is due to the microbial regeneration exceeding the heterotrophic bacterial consumption
374 (Hansell and Orellana, 2021), or it attributes to allochthonous sources from rivers (Bauer and Druffel, 1998). Nutrient
375 distribution and concentrations in the surface layer show significant variability among phases (Fig. 3F, G, and H) due to the
376 varied influence by nutrient-rich upwelling events (predominantly observed in spring-summer), biological assimilation and
377 river discharge. These variations significantly affect the N:P and Si:N ratios (Fig. 3I and J), potentially influencing
378 phytoplankton composition. During winter (Phase III), the N:P ratio approaches the expected Redfield stoichiometry, attributed
379 to reduced denitrification in bottom waters (Fernandez et al., 2015) and limited vertical advection towards the surface,
380 contrasting with Phase I. Simultaneously, the Si:N ratio increases due to freshwater discharge from the Itata River (Phase III),
381 encouraging an increase in large diatoms and subsequent Si(OH)₄ consumption (Phase I). Considering that hot moments occur
382 throughout different phases and stages of primary production, as well as phytoplankton composition succession (Collado-
383 Fabbri et al., 2011; Aldunate et al., 2018; Anabalón et al., 2007), various levels of Chl-a a (see Table 2), and under different
384 nutrient ratios and DOC concentrations (Table 2), it suggests that the conditions and processes favouring the occurrence of hot
385 moments are variables and not entirely clear.

386 The correlation analysis in the water column showed no significant correlations between CH₄ and the other physicochemical
387 variables (Fig. S3A), however nutrients such as PO₄⁻³ were significantly correlated with T (negative correlation), S (positive
388 correlation), DO (negative correlation) and Si:N ratio (positive correlation) (Fig. S3A), which may be associated with the
389 nutrient-rich, oxygen-poor of the ESSW. When the surface layer was analyzed in the three productivity periods (Fig. S3B, C
390 and D), again, no correlation was observed between CH₄ and the other biogeochemical variables, however, in the phase I and
391 II, significant correlations are observed between the nutrients and T, S and DO (negative correlations) (Fig. S3B and C), which
392 may be associated with the upwelling during spring-summer. In the phase III (Fig. S3D), only Si(OH)₄ showed significant

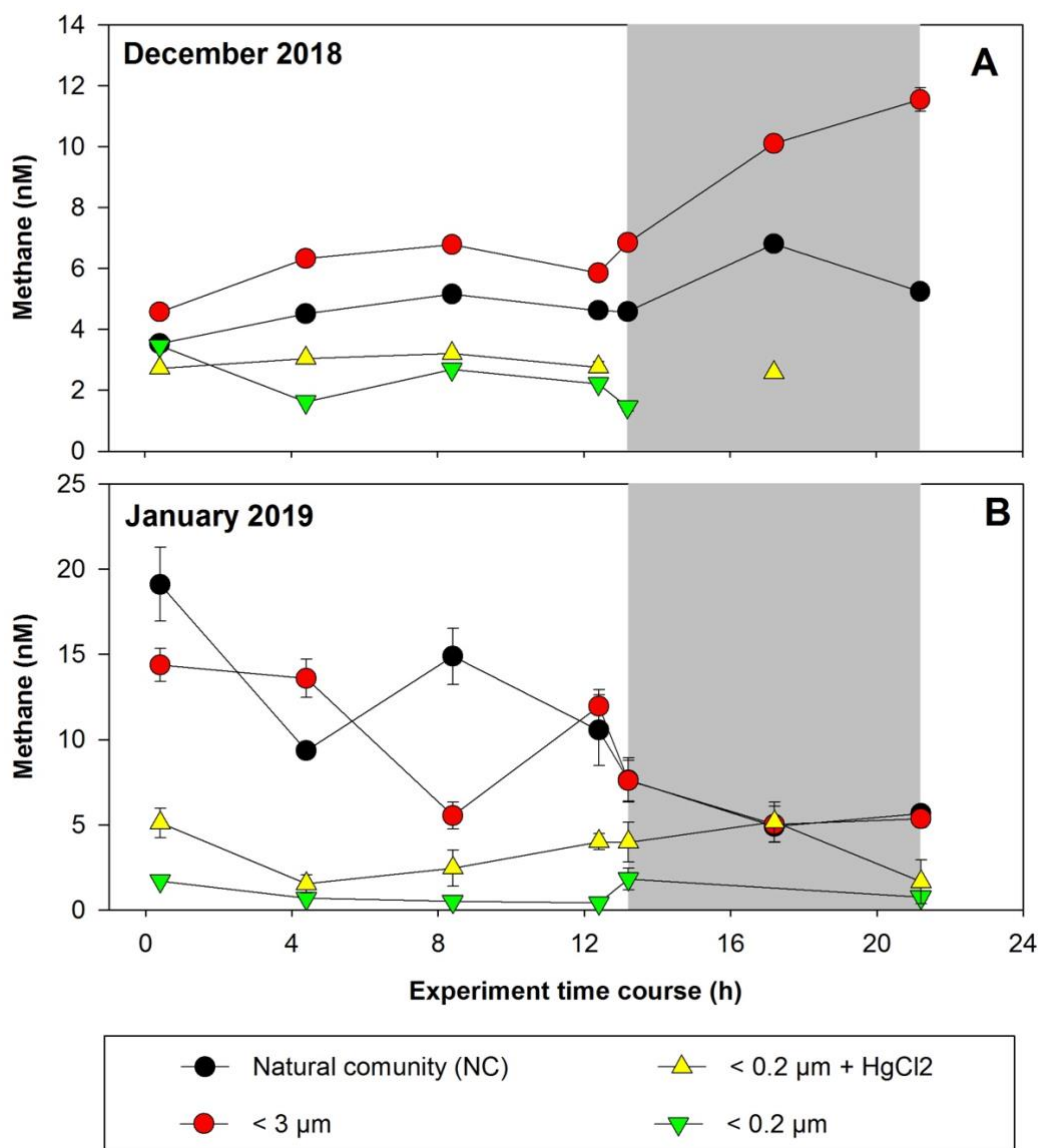
393 correlations with T (negative correlation), NO_3^- (positive correlation), PO_4^{3-} (positive correlation) and the Si:N ratio (positive
394 correlation), this may be due to Si input during the rainfall period presented in the autumn-winter period. Moreover, the slight
395 correlation (but no significant) between CH_4 and Chl-a in Phase III, suggests the possibly organic matter
396 degradation/consumption could impact CH_4 production and that low scale processes (order of hours or days) could mask this
397 correlation, since there is a wide range in the composition of the phytoplankton species are involved in CH_4 cycling (Klitzsch
398 et al., 2019, 2023; Günthel et al., 2020).

399 We further explore the multivariate relationship between CH_4 variability and other variables by separating the data into the
400 surface and subsurface layers by performing a PCA (Fig. S4). Although the CH_4 vector contributes minimally to the total
401 variance in the dataset, distinct behaviour is observed in both layers (Fig. S4A and B). In the surface layer, Principal Component
402 1 (PC1) shows almost no variability in CH_4 and accounts for 25% of the total variance. PC2 contains 22.1% of the total
403 variance and reveals a direct relationship between CH_4 and the variables Chl-a, primary production, Si:N ratio, Si(OH)_4 , PO_4^{3-}
404 3 , and NO_3^- , while being negatively correlated with temperature, DO, NO_2^- , and N:P ratio. When separating dataset into phases,
405 there are differences in variability and the components (Fig. S4C and D). Surface variability is highest in Phase I and lowest
406 in Phase III. Phases I and II vary on both axes, while Phase III is mainly contained on PC2 (Fig. S4C). For the subsurface, the
407 variability is similar in all phases, but the components on which the variability occurs are more differentiated. Phase III varies
408 almost exclusively in the first dimension (the point cloud aligns along the x-axis), while Phases I and II vary on both dimensions
409 (the point cloud is oblique to the axes) (Fig. S4D), this may be due to the differentiation between the upwelling (Phases I and
410 II) and non-upwelling (Phase III) periods.

411 So, the complexity inherent in CH_4 dynamics within the study area poses a challenge to comprehension. Consequently, both
412 short- and long-term CH_4 cycling experiments have been conducted to enhance our understanding. These experiments
413 specifically target size-fractionated planktonic communities combined with organic substrates. The objective is to unravel the
414 intricate interactions and substrates that potentially influence CH_4 production. By focusing on size fractions within planktonic
415 communities, it is possible to assess the contribution of diverse groups to CH_4 production.

416 **3.2 Short-term CH_4 cycling within size fractionated planktonic communities.**

417 Figure 4 shows CH_4 accumulation/depletion in plankton-fractionated experiments over a timeframe, with daily incubations
418 (12 hours of light and 12 hours of darkness). Initial experiments were conducted in December 2018 (Fig. 4A) and January
419 2019 (Fig. 4B), corresponding to a period of high productivity or Phase I (Table S1) and coinciding with strong vertical
420 advection. The surface water exhibits cooling ($\sim 12\text{--}13^\circ\text{C}$) and elevated CH_4 levels (9.44–17.09 nM), indicative of an active
421 upwelling period (Farías et al., 2021), aligning with other indicators of coastal upwelling (Aguirre et al., 2021).



422

423

424

425

426

Figure 4. Time courses of dissolved methane concentration (nM) during incubations with fractionated plankton experiments (NC: natural community; <3 μm: picoplankton and controls (<0.2 μm). A. December 2018 and B. January 2019. Photoperiod is represented in white (light) and gray (dark). Error bars represent standard deviation of triplicate samples, when error bars are not visible, they are within the area of the symbol.

427

428

429

430

In the treatments involving fractions <0.2 μm and <0.2 μm + HgCl₂, which serve as negative controls, CH₄ concentrations remain relatively constant during incubation, with concentrations below 2.32 nM (Fig. 4A) and 5.51 nM (Fig. 4B), indicating biological CH₄ production (Table S2). However, abiotic CH₄ production via photooxidation of CDOM may occur (Li et al., 2020; Zhang and Xie, 2015), but this is not considered in this study. Processes such as DOM photochemical reactions (Mopper

431 et al., 2015), which can contribute to the DOM pool at shallower depths (<10 m) and be photo-oxidized to produce CH₄, are
432 disregarded under natural conditions (Li et al., 2020; Zhang and Xie, 2015). In December, CH₄ concentrations in the NC
433 (positive control) and <3 μm fractions undergo slight increases under light conditions (Fig. 4A, Table S2). However, during
434 darkness, the net CH₄ accumulation is significantly higher in the <3 μm fraction (p = 0.03; Table S2). Picoplankton includes
435 autotrophic and heterotrophic unicellular organisms in the size range of 0.2 to 2 μm. The autotrophic organisms comprise of
436 cyanobacteria (*Prochlorococcus* and *Synechococcus*) and diverse picoeukaryotes larger than 1 μm (Worden, 2006), while the
437 heterotrophic organisms are primarily prokaryotes, with bacteria overwhelmingly dominating over archaea in the upper layers
438 (Smith et al., 2013). This fraction (<3 μm) includes several coexisting metabolic groups that depend on different energy sources
439 such as sunlight, DOC, or even a combination of the two (mixotrophy). These groups are critical for the functioning of the
440 microbial food web and are predominantly responsible for DOC cycling (Muñoz-Marín et al., 2020; Reintjes et al., 2020) and
441 its derivative compounds (including CH₄).

442 In January, the experiments show distinct results, with CH₄ levels decreasing over incubation time in both the NC and <3 μm
443 fractions for both photoperiods (Fig. 4B), although the rate of consumption is lower in darkness (Table S2). These differences
444 suggest that the composition of the microbial community during the high productivity period, as well as the quantity and
445 quality of DOC and nutrient concentrations and their ratios (Allen et al., 2012; Spilling et al., 2019), control CH₄ cycling.
446 Indeed, the environmental conditions differ during sampling (Table S1); although both months are oxygenated, both vary in
447 Chl-a and nutrient levels, including CH₄ (Fig. 3C; Table S1).

448 Significant differences in CH₄ accumulation rates between the NC and <150 μm fraction treatments (data not shown) are
449 observed compared with the <3 μm fraction (Table S2). Peak cycling rates occur in the <3 μm fraction, indicating that larger
450 microorganisms do not affect the net CH₄ accumulation/consumption (Table S2), highlighting the importance of the microbial
451 loop in CH₄ cycling. Additionally, the observed differences between photoperiods in both fractions may suggest coupling
452 mechanisms between autotrophic phytoplankton and heterotrophic bacterioplankton communities (León-Palmero et al., 2020;
453 Morán et al., 2002; Repeta et al., 2016).

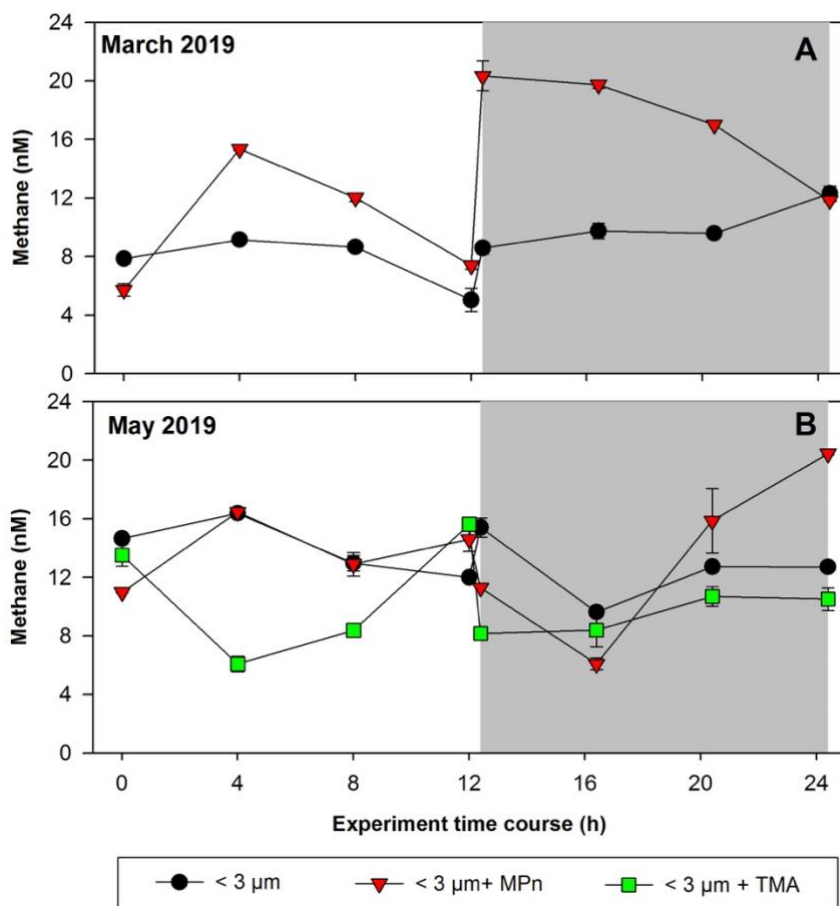
454 CH₄ consumption by methanotrophs should be considered in CH₄ cycling experiments, as aerobic CH₄ oxidation significantly
455 reduces the net CH₄ accumulation rates (net production vs. consumption) (Mao et al., 2022). While the impact of light on
456 methanotrophs is not widely understood (Broman et al., 2023), existing literature suggests that methanotrophs may experience
457 inhibition under light conditions (Dumestre et al., 1999; Morana et al., 2020). Consequently, CH₄ accumulation should be
458 higher under these conditions. However, this does not agree with our results (for light/dark conditions), indicating that
459 methanotrophs are more dynamic and complex than expected, making them difficult to understand through the observation of
460 their daily cycles.

461 **3.3 Short-term CH₄ cycling experiment from picoplankton amended with organic substrates.**

462 As the picoplankton fraction showed the highest rate of CH₄ accumulation (Fig. 4), this prompts its selection for assessing its
463 potential for methylo-trophic methanogenesis through the addition of methylated substrates (MPn and TMA) in a daily cycle.

464 Phosphonate (MPn) and methylamines compounds (mono, di and trimethylamines) are dissolved methylated compounds
465 known to stimulate CH₄ production because they have a methyl radical (-CH₃), a potential precursor for CH₄ formation in
466 oxygenated environments (Karl et al., 2008; Repeta et al., 2016; Wang et al., 2021; Bižić-Ionescu et al., 2018).
467 These compounds are ubiquitous in various ecosystems (Lohrer et al., 2020; Sun et al., 2019), yet they have distinct metabolic
468 origins. The MPn originates from microorganisms as Archaea *Nitrosopumilus maritimus* (Metcalf et al., 2012) and *Candidatus*
469 *pelagibacter spp.* (Born et al., 2017), two of the most abundant marine microorganisms. MPn is found at very low
470 concentrations (~0.01 μM, close to its analytical detection limit) likely due to rapid microbial turnover (Karl et al., 2008;
471 Martínez et al., 2013; Urata et al., 2022). The methylamines compounds as the trimethylamine compounds exhibit a wide
472 concentration range in the ocean, from nM levels in the open ocean to μM levels in sediments and near the coast (Sun et al.,
473 2019). Environmental TMA concentrations could be higher, particularly in upwelling regions that bring the TMA from bottom
474 waters to the surface (Gibb et al., 1999; Sun et al., 2019). In this context, the amendments performed for each substrate, 100-
475 fold for MPn and 1000-fold for TMA, convert these experiments into potential rates.

476 These amendment experiments were conducted in Phase II (March 2019) and Phase III (May 2019), periods of change in
477 phytoplankton succession (composition), biomass and abundance (Testa et al., 2018). In winter, the relative abundance of
478 picoplankton with respect to microplankton (particularly the presence of *Synechococcus* and nitrifying archaea) increases
479 significantly, especially photosynthetic picoeukaryotes (Collado-Fabbri et al., 2011). The time course CH₄ accumulation
480 during incubations is illustrated in Fig. 5. We observe highly variable temporal fluctuations during these periods (March and
481 May). A particularity is the is the abrupt increase in CH₄ concentration upon transitioning from light to dark cycles in March
482 (Phase II), as well as the significant CH₄ accumulation that persists in darkness (Fig. 5A). In May (Phase III), the time course
483 distribution of CH₄ in each treatment exhibits considerable variability. Notably, the addition of MPn results in greater
484 accumulation in CH₄, particularly in darkness, accompanied by a pronounced increase over incubation time (Fig. 5B; Table
485 S2). In both periods, the <3 μm + MPn treatment exhibits contrasting patterns under dark conditions (Fig. 5A and 4B),
486 decreasing in Phase II, and increasing in Phase III, suggesting the importance of microbial composition. During winter (Phase
487 III), a higher DOC concentration is found (Fig 3E), which may lead to higher bacterial and archaeal activity that could be
488 metabolizing DOC, including MPn under dark conditions. On the other hand, despite a coefficient of variation <10%, we
489 cannot entirely discount experimental issues in the abrupt rise of the <3 μm + MPn treatment at around 12 hours.



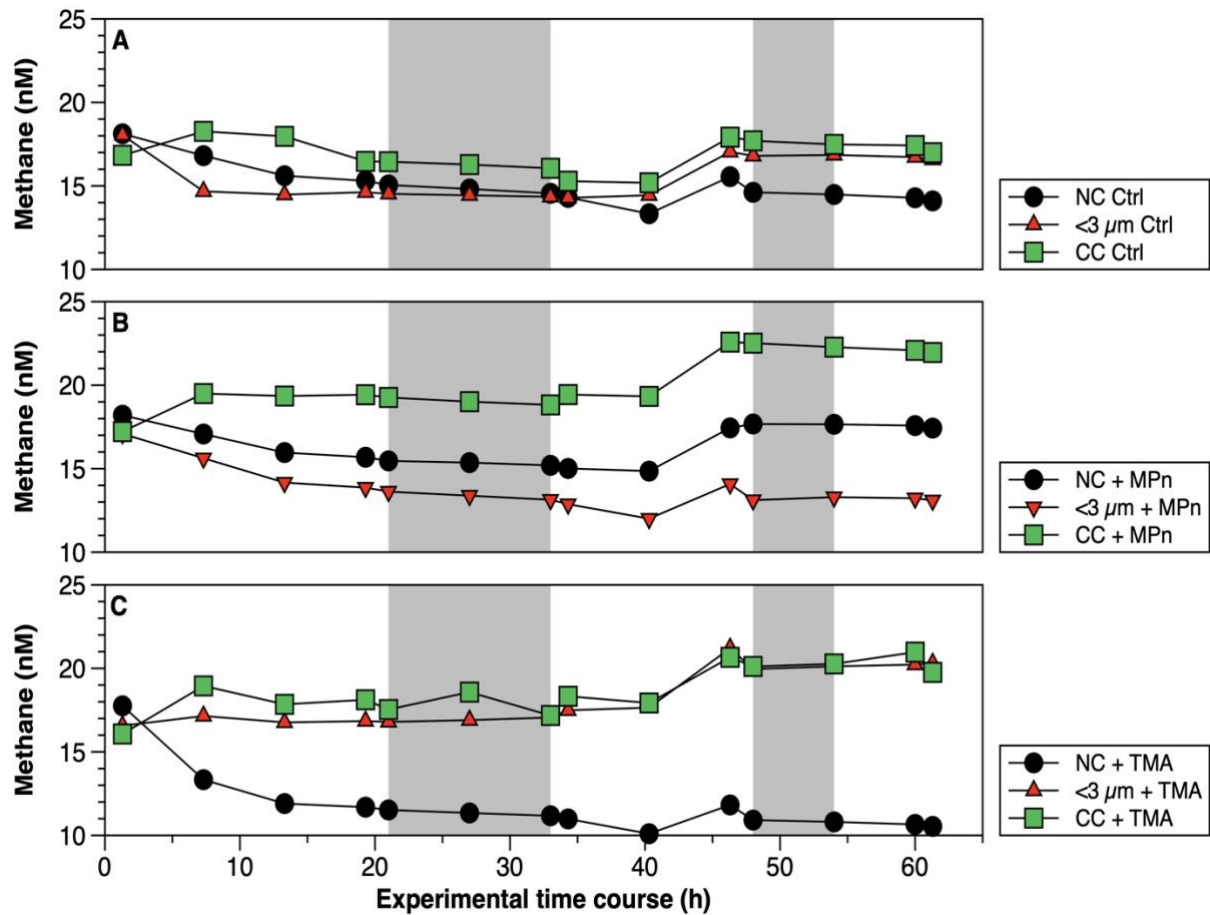
490
 491 **Figure 5.** Time courses of dissolved methane concentration (nM) during incubations with the addition of methylated substrates
 492 (MPn: methyl phosphonic acid and TMA: trimethylamine) performed with bacterioplankton (<3 μm) and bacterioplankton
 493 concentrate (CC). A. March 2019 and B. May 2019. Photoperiod is represented in white (light) and gray (dark). Error bars represent
 494 standard deviation of triplicate samples, when error bars are not visible, they are within the area of the symbol.

495 Conversely, the TMA treatment does not result in any CH₄ accumulation, being lower compared to the control and MPn
 496 treatments (Fig. 5B); while TMA can be metabolized by marine bacteria (Lidbury et al., 2015; Bižić-Ionescu et al., 2018), the
 497 reduced CH₄ production in this treatment suggests an end product different than CH₄ (Sun et al., 2019). In contrast,
 498 heterotrophic picoplankton might metabolize MPn and produce CH₄, showing *in situ* methanogenesis via the carbon-
 499 phosphorus (C-P) lyase pathway (Karl et al., 2008).

500 3.4 Long-term CH₄ cycling from concentrated picoplankton amended with organic substrates.

501 For a more comprehensive understanding, our study involves long-term microcosm experiments conducted during two distinct
 502 phases of productivity. One of these phases occurs during intermediate productivity (Phase II or late summer to autumn),

503 characterized by a notable prevalence of autotrophic small diatoms, pico-eukaryotes, and cyanobacteria (*Synechococcus*), in
504 contrast to the high productivity period (Phase I or early springtime) (Fig. S5A and D), where large diatoms are predominant
505 (Fig. S5B and E), while heterotrophic bacterioplankton exhibits an almost constant presence in both periods (Fig. S5C and F).
506 These temporal distributions align with well-documented phytoplankton and bacterioplankton patterns in our study area
507 (Aldunate et al., 2018; Collado-Fabbri et al., 2011; De La Iglesia et al., 2020; Molina et al., 2020).
508 Briefly, Flavobacteraceae, SAR11 subclade IA (*Candidatus Pelagibacter spp.*), SAR11 subclade 1b, gammaproteobacterial
509 clades, and SAR86 are prevalent during upwelling seasons, while during non-upwelling seasons or Phase III, SAR11 subclade
510 II, Marine Actinobacteria, and unclassified Alphaproteobacteria dominate (Aldunate et al., 2018). In addition, photosynthetic
511 picoplankton eukaryotes related to Mamiellophyceae (*Bathycoccus*, *Micromonas*, and *Ostreococcus*) are predominantly
512 observed with high significance in the surface layer during the transition period (Collado-Fabbri et al., 2011; De La Iglesia et
513 al., 2020), whereas the abundance of heterotrophic bacteria, ranging from 0.23 to 6.50 x10⁶ cells mL⁻¹, is mainly concentrated
514 in the surface during late summer and autumn, with minima in winter (Molina et al., 2020). However, in our study, the
515 abundance of heterotrophic bacteria shows no significant differences (p = 0.05) in both periods (1 x 10⁶ cells mL⁻¹) (Fig. S5C
516 and F). This is due to the low DOC at the beginning of the upwelling period (Fig. 3E).
517 The CH₄ accumulations during time incubations under different treatments in Phase II are illustrated in Figure 6. Net CH₄
518 cycling rates are detailed in Table S4. Variations are observed when these rates are differentiated between light and dark
519 periods, as well as across different periods or phases of productivity (Table S4). The concentrated community (CC) results in
520 substantial enrichments of cyanobacteria (*Synechococcus*), picoeukaryotes, and heterotrophic bacteria by factors of 1.9, 1.8,
521 and 4.6, respectively, compared to the NC, and factors of 1.8, 1.8, and 6.1, respectively, in relation to the natural <3 μm
522 fraction (Figure S5A, B, and C). In both cases, a significant increase in bacteria is observed (Figure S5C). The microbial
523 abundance proportions in the NC treatment at the beginning of the experiment closely align with field observations (Collado-
524 Fabbri et al., 2011; Anabalón et al., 2007; Morales et al., 2007).
525



526
527
528
529
530

Figure 6. Time courses of dissolved methane (nM) during incubation in long-term microcosm experiments (10L) with the addition of methylated substrates (MPn: methyl phosphonic acid and TMA: trimethylamine) performed with three planktonic communities (NC: natural community; <3 μm: bacterioplankton and CC: community concentrate) under oxygenated conditions in April 2019. Photoperiod is represented in white (light) and gray (dark).

531
532
533
534
535
536
537
538
539
540

Mean Chl-a levels in the <3 μm fraction are 21.7 and 4.5 times lower than in the NC and CC, respectively (Table S3). This suggests that this fraction contains phyto-picoeukaryotes (e.g., coccolithophorids, cryptophytes) and picocyanobacteria (e.g., *Synechococcus*) in a lower proportion than the CC. Additionally, the CC treatment displays higher background levels of DOC and nutrients probably due to the natural diurnal mortality of picoplankton (Llabrés et al., 2011). It cannot be ruled out that the baseline is due to tangential flow filtration, although it is one of the most used methods to concentrate DOM (Benner et al., 1992), reducing the amount of membrane sorption and fouling (Minor et al., 2014).

In April (Phase II), CH₄ cycling rates consistently exhibit higher values during the dark phase, suggesting a significant involvement of heterotrophic bacterioplankton (Table S4). Additionally, these rates are notably elevated in the CC treatments, particularly in the CC + MPn (Table S4). When comparing the treatments (NC, <3 μm, and CC) without (controls) and with the addition of MPn and TMA (Fig. 6, Table S4), although temporal patterns are similar, significant differences between

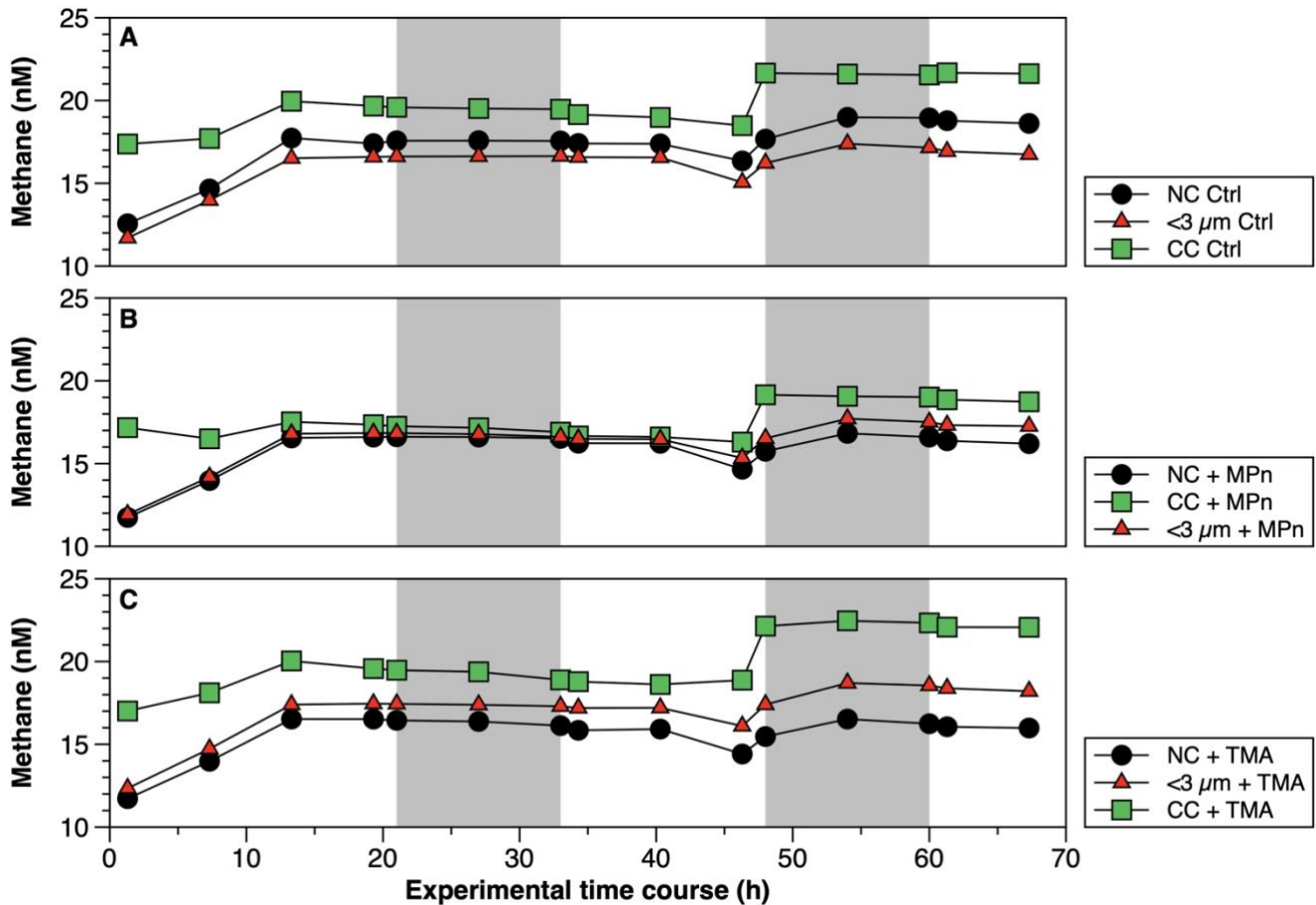
541 treatments ($p = 0.002$) are found with slightly higher CH_4 cycling rates in $<3 \mu\text{m}$ in dark conditions (Fig. 6A; Table S4). With
542 the addition of MPn (Fig. 6B, Table S4), the CC + MPn treatment, characterized by the highest abundance of autotrophic
543 (cyanobacteria) and heterotrophic microorganisms (Fig. S5), exhibits a significant increase in a net CH_4 accumulation in both
544 light and dark conditions (Table S4). In addition, higher Chl-a concentrations (Table S3) in the NC treatment may have
545 supported greater CH_4 accumulation compared to the $<3 \mu\text{m}$ fraction (Fig. 6B). Regarding the TMA enrichment (Fig. 6C),
546 both the CC and the $<3 \mu\text{m}$ fraction treatments respond similarly, increasing CH_4 concentration over time ($p = 3 \times 10^{-6}$; Fig. 6C)
547 although the recycling rates were slightly higher in $<3 \mu\text{m} + \text{TMA}$, suggesting that microbial abundance does not significantly
548 affect CH_4 production with TMA or that the heterotrophic community in the CC treatment weakly metabolizes TMA (De
549 Angelis and Lee, 1994; Bižić-Ionescu et al., 2018).

550 Although the metabolization of methylated substrates, such as MPn to CH_4 by various types of bacteria, has been extensively
551 documented (Repeta et al., 2016; Del Valle and Karl, 2014; Metcalf et al., 2012; Zhao et al., 2022; Damm et al., 2010; Karl et
552 al., 2008), this has only been reported mostly under phosphorus-starved conditions. However, this is unlikely in our study area,
553 which experienced high PO_4^{3-} availability, even in excess compared to N (Table 2). Specifically, the expression of phosphonate
554 C-P lyase genes could arise when P-starved (Carini et al., 2014; Taenzer, 2019; Sosa et al., 2019). Thus, an alternative
555 explanation for the significant CH_4 accumulation in the CC with MPn treatment could be related to the presence of
556 photosynthetic cyanobacteria (Bižić et al., 2020), which have adaptive strategies to fluctuating P levels (Li and Dittrich, 2019).
557 This is further complemented by the capacity of some bacteria to degrade phosphonates in environments with a substantial
558 background of P (Schowanek and Verstraete, 1990).

559 Given that *Synechococcus* dominates during the non-upwelling period (autumn-winter season) in the photic layer (Collado-
560 Fabbri et al., 2011), it becomes plausible to consider CH_4 production mediated by this microorganism in this period.
561 Consequently, CH_4 production pathways appear multifaceted, involving complex interplays between photochemical and
562 metabolic processes. The mechanism by which cyanobacteria effectively convert fixed CO_2 to CH_4 under light conditions
563 appears intricately linked to the photosynthetic process (Bižić et al., 2020; Klintzsch et al., 2020) as inhibitors of photosynthesis
564 blocked CH_4 production under light conditions (Bižić et al., 2020). They suggest that distinct mechanisms might govern CH_4
565 production under light and dark conditions, influenced by freshly synthesized photosynthetic products in light and storage
566 compounds during darkness.

567 In September (Phase I), CH_4 cycling rates exhibit substantial differences compared to those estimated for Phase II. Notably,
568 these rates are lower in most treatments, with a reversal observed in the pattern compared to Phase II, i.e., CH_4 cycling rates
569 during light condition surpass those during dark condition (Table S4). Furthermore, the CC treatments consistently demonstrate
570 the highest rates compared to the other treatments (Table S4). Temporal CH_4 accumulation in this phase, consistently
571 demonstrates higher CH_4 levels in the CC treatment compared to the NC and $<3 \mu\text{m}$ fraction (controls) (Fig. 7A). However, a
572 noteworthy contrast appears when considering the impact of substrate additions. Specifically, the addition of TMA in the CC
573 treatment in this phase results in a more pronounced CH_4 production (Fig. 7C) compared to the effect of MPn (Fig. 7B),
574 especially in dark conditions (Table S4). This pattern, the opposite of that found in Phase II, could potentially be explained by

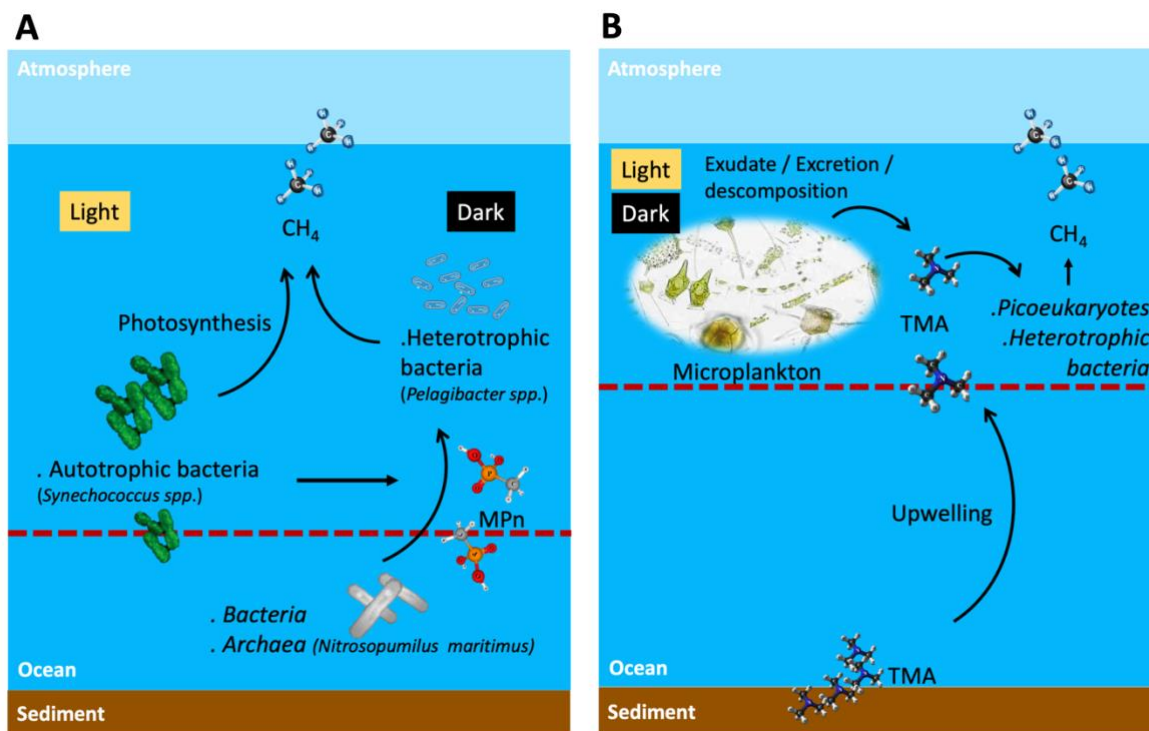
575 the observed decrease in *Synechococcus* abundance (Fig. S5D), which remains unresponsive to MPn, and the concurrent
 576 increase in nano and picoeukaryotes and bacteria at the end of the experiment (Fig. S5E and F); the last of which could be
 577 conducive to the action of TMA (Bižić-Ionescu et al., 2018; De Angelis and Lee, 1994; Lidbury et al., 2015). Indeed, a marked
 578 reduction in *Synechococcus* abundance is observed (showing a 4.6-fold decrease) compared to the Phase II (Fig. S5A and D),
 579 whereas nano- and picoeukaryotes experience notable abundance (3.1 to 3.7 times higher than the transition period) (Fig. S5B
 580 and E).
 581



582
 583 **Figure 7. Time courses of dissolved methane (nM) during incubation in long-term microcosm experiments (10L) with the addition**
 584 **of methylated substrates (MPn: methyl phosphonic acid and TMA: trimethylamine) performed with three planktonic communities**
 585 **(NC: natural community; <3 μm: bacterioplankton and CC: community concentrate) under oxygenated conditions in September**
 586 **2019. Photoperiod is represented in white (light) and gray (dark).**

587 In this phase, the distribution proportions within the NC treatment are cyanobacteria, nano and picoeukaryotes, and bacteria
 588 accounted for 1.1, 2.3 and 96.6, respectively. In contrast, within the CC treatment, the initial distribution proportions are higher
 589 with respect to the NC: cyanobacteria, picoeukaryotes, and bacterioplankton displayed proportions 1.6, 0.6, and 2.9 times

590 greater, respectively. This underscores the increased significance of bacteria and autotrophic picoeukaryotes during this phase,
 591 as further corroborated by Chl-a measurements (Table S3). An intricate interplay between microbial communities and CH₄
 592 cycling within distinct phases of productivity is schematically illustrate in Figure 8. The prevalence of cyanobacteria,
 593 picoeukaryotes, and heterotrophic bacteria varied significantly between these phases. So, this indicates that substrate utilization
 594 is related to the availability of nutrients as well as the complexity of the substrate and the composition of the heterotrophic
 595 bacterial community, potentially driving CH₄ production dynamics.
 596



597
 598 **Figure 8. Suggested scheme of methane cycling mechanisms in two contrasting periods of primary production and oceanographic**
 599 **conditions during light and dark phases, where potential planktonic communities and methylated substrates are involved to**
 600 **metabolize methane in surface waters. A. Phase II and III or late upwelling or non-upwelling season and B. Phase I or active**
 601 **upwelling season. Dashed line shows the 100 μmol L⁻¹ oxycline, above this line oxic methane is produced. TMA: trimethylamine;**
 602 **and MPn: methyl phosphonic acid.**

603 High CH₄ levels in surface water during the non-upwelling period, comparable to the upwelling period, could result from in
 604 situ CH₄ production mediated by photosynthetic *Synechococcus* or demethylation by heterotrophic bacteria (Fig. 8A). On the
 605 other hand, although the trimethylamine methyltransferase enzyme has been described as involved in the demethylation of
 606 TMA in methanogen microorganisms (Paul et al., 2000), it cannot be ruled out that in Phase I (spring) heterotrophic bacteria
 607 dominance can metabolize TMA through an alternative pathway still unknown (Fig. 8B), nor can it be ruled out that the
 608 upwelling brings methanogens with the necessary machinery to metabolize TMA at the ocean surface.

609 4 Conclusions

610 Overall, picoplankton produced CH₄ in all experiments conducted in both light and dark conditions, although the net CH₄
611 production rate was higher in dark conditions. Moreover, laboratory experiments demonstrated that organic compounds such
612 as TMA and MPn are metabolized by heterotrophic bacterioplankton, contributing to the production of oxic CH₄ in the
613 oxygenated surface layer.

614 Coastal upwelling could bring with it organic amino compounds such as TMA including mono and di trimethylamines from
615 sediments, which added to plankton decomposition compounds, and change in picoplanktonic composition (bacteria and the
616 remarkable increase of pico- and nano eukaryotes) during the favorable upwelling period, could promote CH₄ production via
617 TMA, through a pathway that is still unknown, but would potentially add to CH₄ supersaturation in the oxygenated surface
618 layer, beyond the contribution of CH₄ by advection.

619 *Synechococcus* could be responsible for CH₄ regeneration through photosynthesis. These cyanobacteria are abundant in the
620 non-upwelling period, and together with other picoeukaryotes, maintain intermediate and basal Chl-a levels during this period
621 that matched with higher DOC levels and inorganic N:P ratios (compared to the upwelling period). This may stimulate
622 heterotrophic bacteria to metabolize MPn and thus contribute to the recycling of oxic CH₄.

623 It is important to note that amended experiments were conducted in Phase II (March 2019) and Phase III (May 2019), periods
624 marked by changes in the phytoplankton succession (composition), biomass and abundance in winter, the relative abundance
625 of picoplankton with respect to microplankton (particularly the presence of *Synechococcus* and *nitrifying archaea*) increases
626 significantly, especially photosynthetic picoeukaryotes.

627 **Acknowledgements** Thanks to Gerardo Garcia for his experience and teaching in the use of laboratory equipment and his help
628 in setting up the experiments; and Karen Sanzana for nutrient analysis; Oliver Alarcon for oxygen analysis. Both the crew of
629 R/V Kay Kay (II) and the Dichato Marine Station of the University of Concepcion provided valuable help during fieldwork,
630 as well as all participating colleagues in the time series station (University of Concepcion), who provided the core
631 measurements. We also appreciate the work done during the COVID pandemic by Juan Faúndez. This research was funded
632 by the Fondo Nacional de Investigaciones Científicas y Tecnológicas (FONDECYT) grant N° 1200861 and also
633 Millennium Science Initiative Program ICM 2019-015 (SECOS) and CR2 FONDAP-CONICYT N° 1522A001.

634

635 **References**

- 636 Aguirre, C., Pizarro, Ó., Strub, P. T., Garreaud, R., and Barth, J. A.: Seasonal dynamics of the near-surface alongshore flow
637 off central Chile, *J Geophys Res Oceans*, 117, <https://doi.org/10.1029/2011JC007379>, 2012.
- 638 Aguirre, C., Garreaud, R., Belmar, L., Farías, L., Ramajo, L., and Barrera, F.: High-frequency variability of the surface ocean
639 properties off central Chile during the upwelling season, *Front Mar Sci*, 8, 1–19, <https://doi.org/10.3389/fmars.2021.702051>,
640 2021.
- 641 Aldunate, M., De la Iglesia, R., Bertagnolli, A. D., and Ulloa, O.: Oxygen modulates bacterial community composition in the
642 coastal upwelling waters off central Chile, *Deep Sea Research Part II Topical Studies in Oceanography*, 156, 68–79,
643 <https://doi.org/10.1016/j.dsr2.2018.02.001>, 2018.
- 644 Allen, L. Z., Allen, E. E., Badger, J. H., McCrow, J. P., Paulsen, I. T., Elbourne, L. D., Thiagarajan, M., Rusch, D. B., Neelson,
645 K. H., Williamson, S. J., Venter, J. C., and Allen, A. E.: Influence of nutrients and currents on the genomic composition of
646 microbes across an upwelling mosaic, *ISME Journal*, 6, 1403–1414, <https://doi.org/10.1038/ismej.2011.201>, 2012.
- 647 Anabalón, V., Morales, C. E., Escribano, R., Varas, A. M., and Varas, M. A.: The contribution of nano- and micro-planktonic
648 assemblages in the surface layer (0-30 m) under different hydrographic conditions in the upwelling area off Concepción,
649 central Chile, *Prog Oceanogr*, 75, 396–414, <https://doi.org/10.1016/j.pocean.2007.08.023>, 2007.
- 650 De Angelis, M. A. and Lee, C.: Methane production during zooplankton grazing on marine phytoplankton, *Limnol. Oceanogr.*,
651 39, 1298–1308, 1994.
- 652 Bange, H. W., Bartell, U. H., Rapsomanikis, S., and Andreae, M. O.: Methane in the Baltic and North Seas and a reassessment
653 of the marine emissions of methane, *Global Biogeochem Cycles*, 8, 465–480, 1994.
- 654 Bauer, J. and Druffel, E.: Ocean margins as a significant source of organic matter to the deep open ocean, *Letter to nature*,
655 392, 482–485, <https://doi.org/10.1038/33122>, 1998.
- 656 Bello, E.: Variabilidad estacional en la descarga de metano disuelto desde un sistema estuarino a la zona marina adyacente, el
657 caso de ríos de la zona central de Chile (río Itata), Universidad de Concepción, 76 pp., 2016.
- 658 Belviso, S., Kim, S. -K., Rassoulzadegan, F., Krajka, B., Nguyen, B. C., Mihalopoulos, N., and Buat-Menard, P.: Production
659 of dimethylsulfonium propionate (DMSP) and dimethylsulfide (DMS) by a microbial food web, *Limnol Oceanogr*, 35, 1810–
660 1821, <https://doi.org/10.4319/lo.1990.35.8.1810>, 1990.
- 661 Benner, R., Dean Pakulski, J., McCarthy, M., Hedges, J. I., Hatcher, P. G., Benner, R., Pakulski, J. D., McCarthy, M., Hedges,
662 J. I., Hatcher, P. G., H van Beest, B. W., Kramer, G. J., and van Santen, R. A.: Bulk chemical characteristics of dissolved
663 organic matter in the ocean, *J. Glinnemann, ibid*, 255, 1561–1564, [https://doi.org/DOI: 10.1126/science.255.5051.1561](https://doi.org/DOI:10.1126/science.255.5051.1561), 1992.
- 664 Berg, A., Lindblad, P., and Svensson, B. H.: Cyanobacteria as a source of hydrogen for methane formation, *World J Microbiol*
665 *Biotechnol*, 30, 539–545, <https://doi.org/10.1007/s11274-013-1463-5>, 2014.
- 666 Bianchi, T. S.: The role of terrestrially derived organic carbon in the coastal ocean: A changing paradigm and the priming
667 effect, <https://doi.org/10.1073/pnas.1017982108>, 6 December 2011.

668 Bizic, M.: Phytoplankton photosynthesis: An unexplored source of biogenic methane emission from oxic environments, *J*
669 *Plankton Res*, 43, 822–830, <https://doi.org/10.1093/plankt/fbab069>, 2021.

670 Bižić, M., Klintzsch, T., Ionescu, D., Hindiyeh, M. Y., Günthel, M., Muro-Pastor, A. M., Eckert, W., Urich, T., Keppler, F.,
671 and Grossart, H. P.: Aquatic and terrestrial cyanobacteria produce methane, *Sci Adv*, 6, 1–10,
672 <https://doi.org/10.1126/sciadv.aax5343>, 2020.

673 Bižić-Ionescu, M., Ionescu, D., Günthel, M., Tang, K. W., and Grossart, H. P.: Oxic methane cycling: new evidence for
674 methane formation in oxic lake water, *Biogenesis of Hydrocarbons*, 1–22, <https://doi.org/10.1007/978-3-319-53114-4>, 2018.

675 Borges, A. V. and Abril, G.: Carbon Dioxide and Methane Dynamics in Estuaries, Elsevier Inc., 119–161 pp.,
676 <https://doi.org/10.1016/B978-0-12-374711-2.00504-0>, 2012.

677 Born, D. A., Ulrich, E. C., Ju, K. S., Peck, S. C., Van Der Donk, W. A., and Drennan, C. L.: Structural basis for
678 methylphosphonate biosynthesis, *Science* (1979), 358, 1336–1339, <https://doi.org/10.1126/science.aao3435>, 2017.

679 Broecker, W. S. and Peng, T. H.: Gas exchange rates between air and sea, *Tellus XXVI*, 1, 21–35,
680 <https://doi.org/10.1111/j.2153-3490.1974.tb01640.x>, 1974.

681 Broman, E., Barua, R., Donald, D., Roth, F., Humborg, C., Norkko, A., Jilbert, T., Bonaglia, S., and Nascimento, F. J. A.: No
682 evidence of light inhibition on aerobic methanotrophs in coastal sediments using eDNA and eRNA, *Environmental DNA*, 5,
683 766–781, <https://doi.org/10.1002/edn3.441>, 2023.

684 Brown, I. J., Torres, R., and Rees, A. P.: The origin of sub-surface source waters define the sea-air flux of methane in the
685 Mauritanian Upwelling, NW Africa, *Dynamics of Atmospheres and Oceans*, 67, 39–46,
686 <https://doi.org/10.1016/j.dynatmoce.2014.06.001>, 2014.

687 Bullister, J. L., Wisegarver, D. P., and Wilson, S. T.: The production of methane and nitrous oxide gas standards for Scientific
688 Committee on Ocean Research (SCOR) Working Group #143, 1–9 pp., 2016.

689 Capelle, D. W. and Tortell, P. D.: Factors controlling methane and nitrous-oxide variability in the southern British Columbia
690 coastal upwelling system, *Mar Chem*, 179, 56–67, <https://doi.org/10.1016/j.marchem.2016.01.011>, 2016.

691 Capone, D. G. and Hutchins, D. A.: Microbial biogeochemistry of coastal upwelling regimes in a changing ocean,
692 <https://doi.org/10.1038/ngeo1916>, September 2013.

693 Carini, P., White, A. E., Campbell, E. O., and Giovannoni, S. J.: Methane production by phosphate-starved SAR11
694 chemoheterotrophic marine bacteria, *Nat Commun*, 5, 1–7, <https://doi.org/10.1038/ncomms5346>, 2014.

695 Carpenter, J.: Do rats and pigeons readily acquire instrumental responses for food in the presence of free food?, *Limnol*
696 *Oceanogr*, 10, 141–143, <https://doi.org/10.3758/BF03209628>, 1965.

697 Carpenter, L. J., Archer, S. D., and Beale, R.: Ocean-atmosphere trace gas exchange, *Chem Soc Rev*, 41, 6473–6506,
698 <https://doi.org/10.1039/c2cs35121h>, 2012.

699 Cerbin, S., Pérez, G., Rybak, M., Wejnerowski, Ł., Konowalczyk, A., Helmsing, N., Naus-Wiezer, S., Meima-Franke, M.,
700 Pytlak, Ł., Raaijmakers, C., Nowak, W., and Bodelier, P. L. E.: Methane-derived carbon as a driver for cyanobacterial growth,
701 *Front Microbiol*, 13, 1–16, <https://doi.org/10.3389/fmicb.2022.837198>, 2022.

702 Cicerone, R. J. and Oremland, R. S.: Biogeochemical aspects of atmospheric methane, *Global Biogeochem Cycles*, 2, 299–
703 327, <https://doi.org/10.1029/GB002i004p00299>, 1988.

704 Collado-Fabbri, S., Vaultot, D., and Ulloa, O.: Structure and seasonal dynamics of the eukaryotic picophytoplankton
705 community in a wind-driven coastal upwelling ecosystem, *Limnol. Oceanogr.*, 56, 2334–2346,
706 <https://doi.org/10.4319/lo.2011.56.6.2334>, 2011.

707 Cuevas, L. A., Daneri, G., Jacob, B., and Montero, P.: Microbial abundance and activity in the seasonal upwelling area off
708 Concepción (~36°S), central Chile: A comparison of upwelling and non-upwelling conditions, *Deep Sea Res 2 Top Stud*
709 *Oceanogr*, 51, 2427–2440, <https://doi.org/10.1016/j.dsr2.2004.07.026>, 2004.

710 Damm, E., Helmke, E., Thoms, S., Schauer, U., Nöthig, E., Bakker, K., and Kiene, R. P.: Methane production in aerobic
711 oligotrophic surface water in the central Arctic Ocean, *Biogeosciences*, 7, 1099–1108, [https://doi.org/10.5194/bgd-6-10355-](https://doi.org/10.5194/bgd-6-10355-2009)
712 2009, 2010.

713 Damm, E., Beszczynska-Möller, T. A., Nöthing, E. M., and Kattner, G.: Methane excess production in oxygen-rich polar water
714 and a model of cellular conditions for this paradox, *Polar Sci*, 9, 327–334, <https://doi.org/10.1016/j.polar.2015.05.001>, 2015.

715 Dinasquet, J., Tirola, M., and Azam, F.: Enrichment of bacterioplankton able to utilize one-carbon and methylated compounds
716 in the Coastal Pacific Ocean, *Front Mar Sci*, 5, 1–13, <https://doi.org/10.3389/fmars.2018.00307>, 2018.

717 Dumestre, J. F., Guézennec, J., Galy-Lacaux, C., Delmas, R., Richard, S., and Labroue, L.: Influence of light intensity on
718 methanotrophic bacterial activity in Petit Saut Reservoir, French Guiana, *Appl Environ Microbiol*, 65, 534–539,
719 <https://doi.org/10.1128/aem.65.2.534-539.1999>, 1999.

720 Farías, L., Graco, M., and Ulloa, O.: Temporal variability of nitrogen cycling in continental-shelf sediments of the upwelling
721 ecosystem off central Chile, *Deep Sea Res 2 Top Stud Oceanogr*, 51, 2491–2505, <https://doi.org/10.1016/j.dsr2.2004.07.029>,
722 2004.

723 Farías, L., Fernández, C., Faúndez, J., Cornejo, M., and Alcaman, M. E.: Chemolithoautotrophic production mediating the
724 cycling of the greenhouse gases N₂O and CH₄ in an upwelling ecosystem, *Biogeosciences*, 6, 3053–3069,
725 <https://doi.org/https://doi.org/10.5194/bg-6-3053-2009>, 2009.

726 Farías, L., Besoain, V., and García-Loyola, S.: Presence of nitrous oxide hotspots in the coastal upwelling area off central
727 Chile: an analysis of temporal variability based on ten years of a biogeochemical time series, *Environmental Research Letters*,
728 10, 1–13, <https://doi.org/10.1088/1748-9326/10/4/044017>, 2015.

729 Farías, L., Tenorio, S., Sanzana, K., and Faundez, J.: Temporal methane variability in the water column of an area of seasonal
730 coastal upwelling: A study based on a 12 year time series, *Prog Oceanogr*, 195, <https://doi.org/10.1016/j.pocan.2021.102589>,
731 2021.

732 Ferderlman, T. G., Lee, C., Pantoja, S., Harder, J., Bebout, B. M., and Fossing, H.: Sulfate reduction and methanogenesis in a
733 Thioploca- dominates sediment off the coast of Chile, *Geochim Cosmochim Acta*, 61, 3065–3079,
734 [https://doi.org/https://doi.org/10.1016/S0016-7037\(97\)00158-0](https://doi.org/https://doi.org/10.1016/S0016-7037(97)00158-0), 1997.

735 Fernandez, C., González, M. L., Muñoz, C., Molina, V., and Farias, L.: Temporal and spatial variability of biological nitrogen
736 fixation off the upwelling system of central Chile (35-38.5°S), *J Geophys Res Oceans*, 120, 3330–3349,
737 <https://doi.org/10.1002/2014JC010410>, 2015.

738 Florez-Leiva, L., Damm, E., Fariás, L., and Farias, L.: Methane production induced by dimethylsulfide in surface water of an
739 upwelling ecosystem, *Prog Oceanogr*, 112–113, 38–48, <https://doi.org/10.1016/j.pocean.2013.03.005>, 2013.

740 Gibb, S. W., Mantoura, R. F. C., Liss, P. S., and Barlow, R. G.: Distributions and biogeochemistries of methylamines and
741 ammonium in the Arabian Sea, *Deep Sea Res 2 Top Stud Oceanogr*, 46, 593–615, [https://doi.org/10.1016/S0967-
742 0645\(98\)00119-2](https://doi.org/10.1016/S0967-0645(98)00119-2), 1999.

743 Giovannoni, S. J., Delong, E. F., Schmidt, T. M., and Pace, N. R.: Tangential flow filtration and preliminary phylogenetic
744 analysis of marine picoplankton, *Appl Environ Microbiol*, 56, 2572–2575, 1990.

745 González, H. E., Menschel, E., Aparicio, C., and Barría, C.: Spatial and temporal variability of microplankton and detritus,
746 and their export to the shelf sediments in the upwelling area off Concepción, Chile (~36°S), during 2002-2005, *Prog Oceanogr*,
747 75, 435–451, <https://doi.org/10.1016/j.pocean.2007.08.025>, 2007.

748 Grasshoff, K., Ehrhardt, M., and Kremling, K.: *Methods of Seawater Analysis*. Second, Second, Re., John Wiley & Sons, Ltd,
749 Deerfield Beach, Florida: Verlag Chemie, 419 pp., <https://doi.org/10.1002/iroh.19850700232>, 1983.

750 Grossart, H. P., Frindte, K., Dziallas, C., Eckert, W., and Tang, K. W.: Microbial methane production in oxygenated water
751 column of an oligotrophic lake, *Proc Natl Acad Sci U S A*, 108, 19657–19661, <https://doi.org/10.1073/pnas.1110716108>,
752 2011.

753 Günthel, M., Donis, D., Kirillin, G., Ionescu, D., Bizic, M., McGinnis, D. F., Grossart, H. P., and Tang, K. W.: Contribution
754 of oxic methane production to surface methane emission in lakes and its global importance, *Nat Commun*, 10,
755 <https://doi.org/10.1038/s41467-019-13320-0>, 2019.

756 Günthel, M., Klawonn, I., Woodhouse, J., Bižić, M., Ionescu, D., Ganzert, L., Kümmel, S., Nijenhuis, I., Zoccarato, L.,
757 Grossart, H. P., and Tang, K. W.: Photosynthesis-driven methane production in oxic lake water as an important contributor to
758 methane emission, *Limnol Oceanogr*, 1–13, <https://doi.org/10.1002/lno.11557>, 2020.

759 Hahn, M. W.: Broad diversity of viable bacteria in “sterile” (0.2 μm) filtered water, *Res Microbiol*, 155, 688–691,
760 <https://doi.org/10.1016/j.resmic.2004.05.003>, 2004.

761 Hansell, D. A. and Orellana, M. V.: Dissolved organic matter in the global ocean: A primer,
762 <https://doi.org/10.3390/gels7030128>, 1 September 2021.

763 Harmsen, M., van Vuuren, D. P., Bodirsky, B. L., Chateau, J., Durand-Lasserre, O., Drouet, L., Fricko, O., Fujimori, S.,
764 Gernaat, D. E. H. J., Hanaoka, T., Hilaire, J., Keramidas, K., Luderer, G., Moura, M. C. P., Sano, F., Smith, S. J., and Wada,
765 K.: The role of methane in future climate strategies: mitigation potentials and climate impacts, *Clim Change*, 163, 1409–1425,
766 <https://doi.org/10.1007/s10584-019-02437-2>, 2020.

767 Hartmann, J. F., Günthel, M., Klintzsch, T., Kirillin, G., Grossart, H. P., Keppler, F., and Isenbeck-Schröter, M.: High
768 spatiotemporal dynamics of methane production and emission in oxic surface water, *Environ Sci Technol*, 54, 1451–1463,
769 <https://doi.org/10.1021/acs.est.9b03182>, 2020.

770 Holmes, E. M., Sansone, F. J., Rust, T. M., and Popp, B. N.: Methane production, consumption, and air-sea exchange in the
771 open ocean: An evaluation based on carbon isotopic ratios, *Global Biogeochem Cycles*, 14, 1–10,
772 <https://doi.org/10.1029/1999GB001209>, 2000.

773 Holm-Hansen, O., Lorenzen, C. J., Holmes, R. W., and Strickland, J. D. H.: Fluorometric determination of chlorophyll, *Journal*
774 *du Conseil International pour L’Exploration de la Mer*, 30, 3–15, <https://doi.org/10.1093/icesjms/30.1.3>, 1965.

775 Igarza, M., Dittmar, T., Graco, M., and Niggemann, J.: Dissolved organic matter cycling in the coastal upwelling system off
776 central Peru during an “El Niño” year, *Front Mar Sci*, 6, 1–17, <https://doi.org/10.3389/fmars.2019.00198>, 2019.

777 IPCC: Climate change 2021: the physical science basis. Working Group I contribution to the IPCC sixth assessment report,
778 Cambridge University Press, 35–144 pp., 2021.

779 Jacob, B. G., Tapia, F. J., Quiñones, R. A., Montes, R., Sobarzo, M., Schneider, W., Daneri, G., Morales, C. E., Montero, P.,
780 and González, H. E.: Major changes in diatom abundance, productivity, and net community metabolism in a windier and dryer
781 coastal climate in the southern Humboldt Current, *Prog Oceanogr*, 168, 196–209,
782 <https://doi.org/10.1016/j.pocean.2018.10.001>, 2018.

783 Kara, A. B., Rochford, P. A., and Hurlburt, H. E.: Mixed layer depth variability over the global ocean, *J Geophys Res Oceans*,
784 108, 1–15, <https://doi.org/10.1029/2000jc000736>, 2003.

785 Karl, D. and Tilbrook, B.: Production and transport of methane in oceanic particulate organic matter, *Nature*, 368, 732–734,
786 1994.

787 Karl, D., Beversdorf, L., Björkman, K., Church, M., Martinez, A., and DeLong, E.: Aerobic production of methane in the sea,
788 *Nat Geosci*, 1, 473–478, <https://doi.org/10.1038/ngeo234>, 2008.

789 Klintzsch, T., Langer, G., Nehrke, G., Wieland, A., Lenhart, K., and Keppler, F.: Methane production by three widespread
790 marine phytoplankton species: release rates, precursor compounds, and relevance for the environment, *Biogeosciences*, 16,
791 4129–4144, <https://doi.org/10.5194/bg-2019-245>, 2019.

792 Klintzsch, T., Langer, G., Wieland, A., Geisinger, H., Lenhart, K., Nehrke, G., and Keppler, F.: Effects of temperature and
793 light on methane production of widespread marine phytoplankton, *J Geophys Res Biogeosci*, 125, 1–16,
794 <https://doi.org/10.1029/2020JG005793>, 2020.

795 Klintzsch, T., Geisinger, H., Wieland, A., Langer, G., Nehrke, G., Bizic, M., Greule, M., Lenhart, K., Borsch, C., Schroll, M.,
796 and Keppler, F.: Stable carbon isotope signature of methane released from phytoplankton, *Geophys Res Lett*, 50, 1–12,
797 <https://doi.org/10.1029/2023gl103317>, 2023.

798 Kock, A., Gebhardt, S., and Bange, H. W. W.: Methane emissions from the upwelling area off Mauritania (NW Africa),
799 *Biogeosciences*, 5, 1119–1125, <https://doi.org/10.5194/bg-5-1119-2008>, 2008.

800 De La Iglesia, R., Echenique-Subiabre, I., Rodríguez-Marconi, S., Espinoza, J. P., Von Dassow, P., Ulloa, O., and Trefault,
801 N.: Distinct oxygen environments shape picoeukaryote assemblages thriving oxygen minimum zone waters off central Chile,
802 *J Plankton Res*, 42, 514–529, <https://doi.org/10.1093/plankt/fbaa036>, 2020.

803 Lamontagne, R. A., Swinnerton, J. W., Linnenbom, V. J., and Smith, W. D.: Methane concentrations in various marine
804 environments, *J Geophys Res*, 78, 5317–5324, <https://doi.org/10.1029/JC078i024p05317>, 1973.

805 Lenhart, K., Klintzsch, T., Langer, G., Nehrke, G., Bunge, M., Schnell, S., and Keppler, F.: Evidence for methane production
806 by the marine algae *Emiliania huxleyi*, *Biogeosciences*, 13, 3163–3174, <https://doi.org/10.5194/bg-13-3163-2016>, 2016.

807 León-Palmero, E., Contreras-Ruiz, A., Sierra, A., Morales-Baquero, R., and Reche, I.: Dissolved CH₄ coupled to
808 photosynthetic picoeukaryotes in oxic waters and to cumulative chlorophyll a in anoxic waters of reservoirs, *Biogeosciences*,
809 17, 1–23, <https://doi.org/10.5194/bg-17-3223-2020>, 2020.

810 Li, J. and Dittrich, M.: Dynamic polyphosphate metabolism in cyanobacteria responding to phosphorus availability, *Environ*
811 *Microbiol*, 21, 572–583, <https://doi.org/10.1111/1462-2920.14488>, 2019.

812 Li, Y., Fichot, C. G., Geng, L., Scarratt, M. G., and Xie, H.: The contribution of methane photoproduction to the oceanic
813 methane paradox, *Geophys Res Lett*, 47, 1–10, <https://doi.org/10.1029/2020GL088362>, 2020.

814 Lidbury, I. D. E. A., Murrell, J. C., and Chen, Y.: Trimethylamine and trimethylamine N-oxide are supplementary energy
815 sources for a marine heterotrophic bacterium: Implications for marine carbon and nitrogen cycling, *ISME Journal*, 9, 760–769,
816 <https://doi.org/10.1038/ismej.2014.149>, 2015.

817 Llabrés, M., Agustí, S., and Herndl, G. J.: Diel in situ picophytoplankton cell death cycles coupled with cell division, *J Phycol*,
818 47, 1247–1257, <https://doi.org/10.1111/j.1529-8817.2011.01072.x>, 2011.

819 Lohrer, C., Cwierz, P. P., Wirth, M. A., Schulz-Bull, D. E., and Kanwischer, M.: Methodological aspects of methylphosphonic
820 acid analysis: Determination in river and coastal water samples, *Talanta*, 211, 1–8,
821 <https://doi.org/10.1016/j.talanta.2020.120724>, 2020.

822 Lu, X., Jacob, D. J., Zhang, Y., Maasackers, J. D., Sulprizio, M. P., Shen, L., Qu, Z., Scarpelli, T. R., Nesser, H., Yantosca,
823 R. M., Sheng, J., Andrews, A., Parker, R. J., Boesch, H., Anthony Bloom, A., and Ma, S.: Global methane budget and trend,
824 2010-2017: Complementarity of inverse analyses using in situ (globalviewplus ch4 obspack) and satellite (gosat) observations,
825 <https://doi.org/10.5194/acp-21-4637-2021>, 25 March 2021.

826 Ma, X., Sun, M., Lennartz, S. T., and Bange, H. W.: A decade of methane measurements at the Boknis Eck Time-series Station
827 in the Eckernförde Bay (Southwestern Baltic Sea), *Biogeosciences Discussions*, 2020, 1–22, <https://doi.org/10.5194/bg-2020-107>, 2020.

829 Mao, S. H., Zhang, H. H., Zhuang, G. C., Li, X. J., Liu, Q., Zhou, Z., Wang, W. L., Li, C. Y., Lu, K. Y., Liu, X. T., Montgomery,
830 A., Joye, S. B., Zhang, Y. Z., and Yang, G. P.: Aerobic oxidation of methane significantly reduces global diffusive methane
831 emissions from shallow marine waters, *Nat Commun*, 13, <https://doi.org/10.1038/s41467-022-35082-y>, 2022.

832 Martínez, A., Ventouras, L. A., Wilson, S. T., Karl, D. M., and DeLong, E. F.: Metatranscriptomic and functional metagenomic
833 analysis of methylphosphonate utilization by marine bacteria, *Front Microbiol*, 4, <https://doi.org/10.3389/fmicb.2013.00340>,
834 2013.

835 McAuliffe, C.: Solubility in water of C1-C9 hydrocarbons, *Nature*, 200, 1092–1093, 1963.

836 McClain, M. E., Boyer, E. W., Dent, C. L., Gergel, S. E., Grimm, N. B., Groffman, P. M., Hart, S. C., Harvey, J. W., Johnston,
837 C. A., Mayorga, E., McDowell, W. H., and Pinay, G.: Biogeochemical Hot Spots and Hot Moments at the Interface of
838 Terrestrial and Aquatic Ecosystems, <https://doi.org/10.1007/s10021-003-0161-9>, June 2003.

839 Metcalf, W. W., Griffin, B. M., Cicchillo, R., Gao, J., Janga, S., Cooke, H., Circello, B., Evans, B., Martens-Habbena, W.,
840 Stahl, D., and Van Der Donk, W.: Synthesis of methylphosphonic acid by marine microbes: a source for methane in the
841 Aerobic Ocean, *Science* (1979), 337, 1104–1107, <https://doi.org/10.1126/science.1219875>, 2012.

842 Minor, E. C., Swenson, M. M., Mattson, B. M., and Oyler, A. R.: Structural characterization of dissolved organic matter: A
843 review of current techniques for isolation and analysis, *Environmental Sciences: Processes and Impacts*, 16, 2064–2079,
844 <https://doi.org/10.1039/c4em00062e>, 2014.

845 Molina, V., Belmar, L., Levipan, H. A., Ramírez-Flandes, S., Anguita, C., Galán, A., Montes, I., and Ulloa, O.: Spatiotemporal
846 distribution of key pelagic microbes in a seasonal oxygen-deficient coastal upwelling system of the Eastern South Pacific
847 Ocean, *Front Mar Sci*, 7, 1–17, <https://doi.org/10.3389/fmars.2020.561597>, 2020.

848 Mopper, K., Kieber, D. J., and Stubbins, A.: Marine photochemistry of organic matter: processes and impacts. processes and
849 impacts., in: *Biogeochemistry of Marine Dissolved Organic Matter: Second Edition*, Elsevier Inc., 389–450,
850 <https://doi.org/10.1016/B978-0-12-405940-5.00008-X>, 2015.

851 Morales, C. and Anabalón, V.: Phytoplankton biomass and microbial abundances during the spring upwelling season in the
852 coastal area off Concepción , central-southern Chile : variability around a time series station, *Prog Oceanogr*, 92–95, 81–91,
853 <https://doi.org/10.1016/j.pocean.2011.07.004>, 2012.

854 Morales, C., González, H. E., Hormazabal, S. E., Yuras, G., Letelier, J., and Castro, L. R.: The distribution of chlorophyll- a
855 and dominant planktonic components in the coastal transition zone off Concepción, central Chile, during different
856 oceanographic conditions, *Prog Oceanogr*, 75, 452–469, <https://doi.org/10.1016/j.pocean.2007.08.026>, 2007.

857 Morán, X. A. G., Estrada, M., Gasol, J. M., and Pedrós-Alió, C.: Dissolved primary production and the strength of
858 phytoplankton-bacterioplankton coupling in contrasting marine regions, *Microb Ecol*, 44, 217–223,
859 <https://doi.org/10.1007/s00248-002-1026-z>, 2002.

860 Morana, C., Bouillon, S., Nolla-Ardèvol, V., Roland, F., Okello, W., Descy, J.-P., Nankabirwa, A., Nabafu, E., Springael, D.,
861 and Borges, A.: Methane paradox in tropical lakes? Sedimentary fluxes rather than water column production in oxic waters
862 sustain methanotrophy and emissions to the atmosphere, *Biogeosciences Discussions*, 17, 1–20, [https://doi.org/10.5194/bg-](https://doi.org/10.5194/bg-2020-142)
863 2020-142, 2020.

864 Muñoz-Marín, M. C., Gómez-Baena, G., López-Lozano, A., Moreno-Cabezuelo, J. A., Díez, J., and García-Fernández, J. M.:
865 Mixotrophy in marine picocyanobacteria: use of organic compounds by *Prochlorococcus* and *Synechococcus*,
866 <https://doi.org/10.1038/s41396-020-0603-9>, 1 May 2020.

867 Oremland, R. S.: Methanogenic activity in plankton samples and fish intestines: A mechanism for in situ methanogenesis in
868 oceanic surface waters, *Limnol. Oceanogr.*, 24, 1136–1141, 1979.

869 Paul, L., Ferguson, D. J., and Krzycki, J. A.: The trimethylamine methyltransferase gene and multiple dimethylamine
870 methyltransferase genes of *methanosarcina barkeri* contain in-frame and read-through amber codons, *J Bacteriol*, 182, 2520–
871 2529, [https://doi.org/0021-9193/00/\\$04.00](https://doi.org/0021-9193/00/$04.00), 2000.

872 Rain-Franco, A., Sobarzo, M., Caparros, J., and Fernandez, C.: Variability of chromophoric dissolved organic matter in three
873 freshwater-influenced systems along central-southern Chile, *Prog Oceanogr*, 174, 154–161,
874 <https://doi.org/10.1016/j.pocean.2018.09.009>, 2019.

875 Raven, J. A.: The twelfth tansley lecture. Small is beautiful: the picophytoplankton, *Funct Ecol*, 12, 503–513,
876 <https://doi.org/10.1046/j.1365-2435.1998.00233.x>, 1998.

877 Reeburgh, W. S.: Oceanic methane biogeochemistry, *American Chemical Society*, 107, 486–513,
878 <https://doi.org/10.1021/cr050362v>, 2007.

879 Reintjes, G., Fuchs, B. M., Scharfe, M., Wiltshire, K. H., Amann, R., and Arnosti, C.: Short-term changes in polysaccharide
880 utilization mechanisms of marine bacterioplankton during a spring phytoplankton bloom, *Environ Microbiol*, 22, 1884–1900,
881 <https://doi.org/10.1111/1462-2920.14971>, 2020.

882 Repeta, D. J., Ferrón, S., Sosa, O. A., Johnson, C. G., Repeta, L. D., Acker, M., DeLong, E. F., and Karl, D. M.: Marine
883 methane paradox explained by bacterial degradation of dissolved organic matter, *Nat Geosci*, 9, 1–7,
884 <https://doi.org/10.1038/ngeo2837>, 2016.

885 Roth, F., Sun, X., Geibel, M. C., Prytherch, J., Brüchert, V., Bonaglia, S., Broman, E., Nascimento, F., Norkko, A., and
886 Humborg, C.: High spatiotemporal variability of methane concentrations challenges estimates of emissions across vegetated
887 coastal ecosystems, *Glob Chang Biol*, <https://doi.org/10.1111/gcb.16177>, 2022.

888 Saunio, M., Stavert, A. R., Poulter, B., Bousquet, P., Canadell, J. G., Jackson, R. B., Raymond, P. A., Dlugokencky, E. J.,
889 and Houweling, S.: The global methane budget 2000 – 2017, *Earth Syst Sci Data*, 12, 1561–1623, [https://doi.org/10.5194/essd-](https://doi.org/10.5194/essd-12-1561-2020)
890 [12-1561-2020](https://doi.org/10.5194/essd-12-1561-2020), 2020.

891 Schlitzer, R.: Ocean Data View, 2023.

892 Schowanek, D. and Verstraete, W.: Phosphonate utilization by bacteria in the presence of alternative phosphorus sources,
893 *Biodegradation*, Kluwer Academic Publishers, 1990 pp., 1990.

894 Sieburth, J., Smetacek, V., and Lenz, J.: Pelagic ecosystem structure: Heterotrophic compartments of the plankton and their
895 relationship to plankton size fractions, *Limnol. Oceanogr.*, 23, 1256–1263, <https://doi.org/10.4319/lo.1978.23.6.1256>, 1978.

896 Smith, M. W., Allen, L. Z., Allen, A. E., Herfort, L., and Simon, H. M.: Contrasting genomic properties of free-living and
897 particle-attached microbial assemblages within a coastal ecosystem, *Front Microbiol*, 4, 1–20,
898 <https://doi.org/10.3389/fmicb.2013.00120>, 2013.

899 Sobarzo, M. and Djurfeldt, L.: Coastal upwelling process on a continental shelf limited by submarine canyons, Concepción,
900 central Chile, *J Geophys Res*, 109, 1–20, <https://doi.org/10.1029/2004JC002350>, 2004.

901 Sobarzo, M., Bravo, L., Donoso, D., Garcés-Vargas, J., and Schneider, W.: Coastal upwelling and seasonal cycles that
902 influence the water column over the continental shelf off central Chile, *Prog Oceanogr*, 75, 363–382,
903 <https://doi.org/10.1016/j.pocean.2007.08.022>, 2007.

904 Sosa, O. A., Repeta, D. J., DeLong, E. F., Ashkezari, M. D., and Karl, D. M.: Phosphate-limited ocean regions select for
905 bacterial populations enriched in the carbon–phosphorus lyase pathway for phosphonate degradation, *Environ Microbiol*, 21,
906 2402–2414, <https://doi.org/10.1111/1462-2920.14628>, 2019.

907 Sosa, O. A., Burrell, T. J., Wilson, S. T., Foreman, R. K., Karl, D. M., and Repeta, D. J.: Phosphonate cycling supports methane
908 and ethylene supersaturation in the phosphate-depleted western North Atlantic Ocean, *Limnol Oceanogr*, 1–17,
909 <https://doi.org/10.1002/lno.11463>, 2020.

910 Spilling, K., Camarena-Gómez, M. T., Lipsewers, T., Martinez-Varela, A., Díaz-Rosas, F., Eronen-Rasimus, E., Silva, N., von
911 Dassow, P., and Montecino, V.: Impacts of reduced inorganic N:P ratio on three distinct plankton communities in the Humboldt
912 upwelling system, *Mar Biol*, 166, 1–17, <https://doi.org/10.1007/s00227-019-3561-x>, 2019.

913 Stefels, J. and Van Boekel, W.: Production of DMS from dissolved DMSP in axenic cultures of the marine phytoplankton
914 species *Phaeocystis* sp, *Mar Ecol Prog Ser*, 97, 11–18, <https://doi.org/https://www.jstor.org/stable/24833593>, 1993.

915 Strub, T., Mesías, J., Montecino, V., Rutllant, J., and Salinas, S.: Coastal ocean circulation off western south america, in: *The*
916 *global coastal ocean - regional studies and syntheses*, vol. 11, 273–313, 1998.

917 Sun, J., Steindler, L., Thrash, J. C., Halsey, K. H., Smith, D. P., Carter, A. E., Landry, Z. C., and Giovannoni, S. J.: One carbon
918 metabolism in SAR11 pelagic marine bacteria, *PLoS One*, 6, 1–12, <https://doi.org/10.1371/journal.pone.0023973>, 2011.

919 Sun, J., Mausz, M. A., Chen, Y., and Giovannoni, S. J.: Microbial trimethylamine metabolism in marine environments, *Environ*
920 *Microbiol*, 21, 513–520, <https://doi.org/10.1111/1462-2920.14461>, 2019.

921 Taenzer, L.: *The isotope biogeochemistry of methane produced from the C-P lyase pathway*, Dartmouth College, 2019.

922 Testa, G., Masotti, I., and Farías, L.: Temporal variability in net primary production in an upwelling area off central Chile
923 (36°S), *Front Mar Sci*, 5, 1–17, <https://doi.org/10.3389/fmars.2018.00179>, 2018.

924 Upstill-goddard, R. C. and Barnes, J.: Methane emissions from UK estuaries: Re-evaluating the estuarine source of
925 tropospheric methane from Europe, 180, 14–23, <https://doi.org/10.1016/j.marchem.2016.01.010>, 2016.

926 Urata, S., Kurosawa, Y., Yamasaki, N., Yamamoto, H., Nishiwaki, N., Hongo, Y., Adachi, M., and Yamaguchi, H.: Utilization
927 of phosphonic acid compounds by marine bacteria of the genera *Phaeobacter*, *Ruegeria*, and *Thalassospira* (α -Proteobacteria),
928 *FEMS Microbiol Lett*, 369, <https://doi.org/10.1093/femsle/fnac065>, 2022.

929 Del Valle, D. A. and Karl, D. M.: Aerobic production of methane from dissolved water-column methylphosphonate and sinking
930 particles in the North Pacific Subtropical Gyre, *Aquatic Microbial Ecology*, 73, 93–105, <https://doi.org/10.3354/ame01714>,
931 2014.

932 Vargas, C. A., Martínez, R. A., Cuevas, L. A., Pavez, M. A., Cartes, C., González, H. E., Escribano, R., and Daneri, G.: The
933 relative importance of microbial and classical food webs in a highly productive coastal upwelling area, *Limnol Oceanogr*, 52,
934 1495–1510, <https://doi.org/10.4319/lo.2007.52.4.1495>, 2007.

935 Vargas, C. A., Arriagada, L., Sobarzo, M., Contreras, P. Y., and Saldías, G.: Bacterial production along a river-to-ocean
936 continuum in central Chile: implications for organic matter cycling, *Aquatic Microbial Ecology*, 68, 195–213,
937 <https://doi.org/10.3354/ame01608>, 2013.

938 Vargas, C. A., Contreras, P. Y., Pérez, C. A., Sobarzo, M., Saldías, G. S., and Salisbury, J.: Influences of riverine and upwelling
939 waters on the coastal carbonate system off Central Chile and their ocean acidification implications, *J Geophys Res Biogeosci*,
940 121, 1–16, <https://doi.org/10.1002/2015JG003213>, 2016.

941 Wang, Q., Dore, J. E., and McDermott, T. R.: Methylphosphonate metabolism by *Pseudomonas* sp. populations contributes to
942 the methane oversaturation paradox in an oxic freshwater lake, *Environ Microbiol*, 19, 1–41, <https://doi.org/10.1111/1462-2920.13747>, 2018.

944 Wang, Q., Alowaifeer, A., Kerner, P., Balasubramanian, N., Patterson, A., Christian, W., Tarver, A., Dore, J. E., Hatzepichler,
945 R., Bothner, B., and McDermott, T. R.: Aerobic bacterial methane synthesis, *Proceedings of the National Academy of*
946 *Sciences*, 118, 1–9, <https://doi.org/10.1073/pnas.2019229118>, 2021.

947 Wanninkhof, R.: Relationship between wind speed and gas exchange over the ocean, *J Geophys Res*, 97, 7373–7382,
948 <https://doi.org/10.1029/92JC00188>, 1992.

949 Weber, T., Wiseman, N. A., and Kock, A.: Global ocean methane emissions dominated by shallow coastal waters, *Nat*
950 *Commun*, 10, 1–10, <https://doi.org/10.1038/s41467-019-12541-7>, 2019.

951 Wiesenburg, D. A. and Guinasso, N. L.: Equilibrium solubilities of methane, carbon monoxide, and hydrogen in water and sea
952 water, *American Chemical Society*, 24, 356–360, 1979.

953 Worden, A.: Picoeukaryote diversity in coastal waters of the Pacific Ocean, *Aquatic microbial ecology*, 43, 165–175,
954 <https://doi.org/doi:10.3354/ame043165>, 2006.

955 Xu, S., Sun, Z., Geng, W., Cao, H., Zhang, X., Zhai, B., and Wu, Z.: Advance in Numerical Simulation Research of Marine
956 Methane Processes, *Front Earth Sci (Lausanne)*, 10, <https://doi.org/10.3389/feart.2022.891393>, 2022.

957 Ye, W. W., Wang, X. L., Zhang, X.-H., and Zhang, G.-L.: Methane production in oxic seawater of the western North Pacific
958 and its marginal seas, *Limnol Oceanogr*, 65, 1–14, <https://doi.org/10.1002/lno.11457>, 2020.

959 Zhang, Y. and Xie, H.: Photomineralization and photomethanification of dissolved organic matter in Saguenay River surface
960 water, *Biogeosciences*, 12, 6823–6836, <https://doi.org/10.5194/bg-12-6823-2015>, 2015.

961 Zhao, L., Lin, L.-Z., Chen, M.-Y., Teng, W.-K., Zheng, L.-L., Peng, L., Lv, J., Brand, J. J., Hu, C.-X., Han, B.-P., Song, L.-
962 R., and Shu, W.-S.: The widespread capability of methylphosphonate utilization in filamentous cyanobacteria and its
963 ecological significance, *Water Res*, 217, 1–11, <https://doi.org/10.1016/j.watres.2022.118385>, 2022.

964